NACA TN 4368

NATIONAL ADVISORY COMMITTEE FOR AERONAUTICS

TECHNICAL NOTE 4368

A STUDY OF SEVERAL THEORETICAL METHODS FOR COMPUTING THE ZERO-LIFT WAVE DRAG OF A FAMILY OF OPEN-NOSED BODIES OF REVOLUTION IN THE MACH NUMBER RANGE OF 2.0 TO 4.0

By Leroy L. Presley and Emmet A. Mossman

Ames Aeronautical Laboratory
Moffett Field, Calif.

NACA

Washington

September 1958

NATIONAL ADVISORY COMMITTEE FOR AERONAUTICS

TECHNICAL NOTE 4368

A STUDY OF SEVERAL THEORETICAL METHODS FOR COMPUTING THE ZERO-LIFT WAVE DRAG OF A FAMILY OF OPEN-NOSED BODIES OF REVOLUTION IN THE MACH NUMBER RANGE OF 2.0 TO 4.0

By Leroy L. Presley and Emmet A. Mossman

SUMMARY

The wave drag of a family of open-nosed bodies of revolution was computed by six approximate theories, first-order perturbation theory, second-order perturbation theory, generalized shock-expansion theory, second-order shock-expansion theory, tangent-wedge theory, and impact theory, and by the method of characteristics for Mach numbers between 2.0 and 4.0. The best agreement with the method of characteristics was provided by second-order perturbation theory and second-order shock-expansion theory with the latter being the most attractive from the standpoint of computing time required versus accuracy obtained.

The wave drag, for bodies of the type investigated in this study with the same initial lip angle and the same diameter ratio (initial to maximum diameter), was found to increase sharply for fineness ratios less than 3 but to be nearly constant for fineness ratios above 3. The wave drag was found to decrease nearly linearly as the diameter ratio increases for bodies having the same initial lip angle and fineness ratio.

An approach is given for adapting the method of characteristics to automatic computing machine procedure.

INTRODUCTION

For aircraft configurations employing a pod-nacelle arrangement to house an air breathing propulsion system, the external wave drag of the engine housing can be a significant portion of the total drag of the aircraft. In the absence of systematic experimental data to aid in estimating this wave drag, the usual approach is to calculate it theoretically. At present there are a number of different theoretical methods which can be used for such calculations. However, the results obtained from the various methods are not consistent over a wide range of Mach numbers and body shapes and the computation time differs widely among the methods. The investigation described herein was made, therefore,

to compare the theoretical wave drag as computed using six approximate methods with that from the method of characteristics in order that a choice from the viewpoint of average computing time required and accuracy obtained could be made. The theories which were compared to the method of characteristics were: first-order perturbation theory (refs. 1 and 2), second-order perturbation theory (ref. 2), generalized shock-expansion theory (refs. 3 and 4), second-order shock-expansion theory (ref. 5), tangent-wedge theory (ref. 6), and impact theory (ref. 7).

To provide a reference for the comparison, the study was conducted for a family of open-nosed bodies of revolution having a fineness ratio of 5, a ratio of initial to maximum diameter of 0.742, and lip angles between 1.478° and 35.844°. This family was selected since its contours are representative of the nacelles of present day pod-nacelle arrangements for jet engines. Thus the wave-drag characteristics of such a family are of interest in themselves. The effects of varying fineness ratio and diameter ratio were also determined using the method of characteristics and generalized shock-expansion theory.

THEORETICAL METHODS

Although the various theoretical methods used in the present study have been discussed in detail in their respective references, it is considered appropriate to this report to discuss briefly each of the methods, pointing out in particular their approach to the solution of the supersonic flow field about an open-nosed body of revolution and their expected range of applicability. All of the theories used in this analysis have as their basis a solution of the gasdynamics equation shown below:

$$\left(1 - \frac{u^2}{a^2}\right)\frac{\partial u}{\partial x} + \left(1 - \frac{v^2}{a^2}\right)\frac{\partial v}{\partial r} - \frac{uv}{a^2}\left(\frac{\partial u}{\partial r} + \frac{\partial v}{\partial x}\right) + \frac{v}{r} = 0 \qquad (1)$$

where the symbols are defined in appendix A. Since this equation, which is applicable to any steady inviscid flow of a perfect gas, is nonlinear, simplified methods of solution must be used for most problems. The simplified methods of solution which have resulted in the theories used in this study are: numerical solution of equation (1), linearization of equation (1) with subsequent analytical solution of the linearized equation, and approximate solutions of equation (1) which are applicable to certain flow regimes. In the application of the theories, the following conditions were imposed:

(1) The flow entered the nose of the body at supersonic speed (i.e., mass-flow ratio of unity).

(2) The bodies were immersed in an ideal gas.

(3) The bodies were at zero angle of attack.

Method of Characteristics

One method of solving the gasdynamics equations is by numerical means. Such a method is greatly facilitated in the present case of supersonic flow since the gasdynamics equation is a hyperbolic differential equation and of a type that is integrable on characteristic surfaces which correspond to Mach lines. It is then necessary to rewrite equation (1) in a form suitable for numerical integration along the Mach lines, and several different forms have been derived (refs. 8, 9, and 10). One form of the compatability equation for the method of characteristics which was considered to be the most satisfactory for the present study since it contains only two flow-field variables is as follows:[1]

$$dp = \mp \lambda\left(d\delta \pm \frac{ds}{r} \sin \mu \sin \delta\right) \tag{2}$$

where

$$\lambda = \frac{2\gamma p}{\sin 2\mu} \tag{3}$$

with the upper sign referring to the first family Mach line and the lower to the second family Mach line as shown in figure 1. Equation (2) expresses the relationship between static pressure, stream angle, and Mach angle along Mach lines in the flow field and is applicable to either rotational or irrotational steady flow of an isoenergetic gas. When applied to rotational flow, as in this study, the change in entropy normal to the streamlines is taken into account by considering the change in total pressure along the Mach lines. This method is limited to bodies with supersonic flow behind the nose shock.

In the actual solution of the flow by the method of characteristics, the compatability equation is put into finite difference form and solved point for point in the flow field. If solved by purely numerical means, the computations are very long and laborious for any practical problems and become feasible only with the use of automatic computing machines.

In the present study, the computations were made using an automatic computing machine. The equations used as well as a discussion of some considerations in the adaption of the method of characteristics to automatic computing machine procedure are given in appendix B.

First-Order Theory

In contrast to the numerical integration of the nonlinear gasdynamics equation by the method of characteristics, first-order theory introduces

[1]This form is not given directly in either references 8, 9, or 10 but can be obtained by a suitable combination of equations 3.21 to 3.23 in Chapter I of reference 10.

a perturbation function into the equation and linearizes the resulting expression so that it may be solved analytically. This is done by considering the magnitude of the velocities in the following manner

$$\begin{aligned} u &= U + u_p & \qquad v &= v_p \\ u_p \text{ and } v_p &\ll U & \qquad u_p \text{ and } v_p &\ll a \end{aligned} \tag{4}$$

and defining a perturbation potential such that

$$u_p = \frac{\partial \varphi}{\partial x} \qquad v_p = \frac{\partial \varphi}{\partial r}$$

Equation (1) can be put into the following form

$$\left[1 - \left(U + \frac{\partial \varphi}{\partial x}\right)^2\right] \frac{\partial^2 \varphi}{\partial x^2} + \left[1 - \left(\frac{\partial \varphi}{\partial r}\right)^2\right] \frac{\partial^2 \varphi}{\partial r^2} + \frac{1}{r} \frac{\partial \varphi}{\partial r} = 2 \frac{\partial \varphi}{\partial x} \frac{\partial \varphi}{\partial r} \frac{\partial^2 \varphi}{\partial x \, \partial r} \tag{5}$$

If the squares and products of derivatives of the perturbation potential are neglected, the following equation results

$$\frac{\partial^2 \varphi}{\partial r^2} - \beta^2 \frac{\partial^2 \varphi}{\partial x^2} + \frac{1}{r} \frac{\partial \varphi}{\partial r} = 0 \tag{6}$$

where $\beta^2 = M^2-1$. Equation (6) is the linearized form of the potential flow equation. Details of the integration of this equation are given in references 1 and 2. Such a solution is applicable to the calculation of flow fields at values of the hypersonic similarity parameter, $M_\infty \delta_o$, less than 1.0. It in effect neglects entropy losses due to the presence of the body since entropy losses are of third order in the perturbation potential.

Second-Order Theory

The third approach to obtaining a solution of equation (1) is to use an iteration procedure, an approach first considered by Busemann and later extended by Van Dyke (ref. 2). For this method, a first-order solution is obtained as described previously. This solution is substituted into the right-hand side of equation (5) and a second-order perturbation potential is found. The method of solution is given in reference 11. Therein it was stated that the initial angularity of the body must be less than the free-stream Mach angle.

In the present study the computations were done using an automatic computing machine since they are lengthy when done by hand. The initial angularity of the bodies was restricted to 13° or less because of the

limitations in the automatic computing machine program, an angle considerably less than that permitted by the theory. This theory is also applied only in the range of $M_\infty\delta_o < 1.0$.

Generalized Shock-Expansion Method

A method which has as its basis an approximate solution of the exact equation of motion is the well-known generalized shock-expansion theory. The approximation made for this theory consists of neglecting the term $(ds/r)\sin\mu \sin\delta$ of equation (2) for cases in which the rate of change of surface angle of the body is large compared to its divergence. The resulting expression is seen to be a differential form of the Prandtl-Meyer equation. The flow field downstream of the nose shock wave can then be considered of the Prandtl-Meyer type. The aforementioned assumption regarding the body shape is made in this theory so it could be expected to become accurate when $M_\infty\delta_o \gg 1.0$ and when the area ratio of the body (maximum to initial area) is near 1.

The application of this method begins by first approximating the body by a series of straight-line elements, tangent to the original body. The flow at the nose is defined by means of the Rankine-Hugoniot relations for an oblique shock wave. Since the flow downstream of the nose is of the Prandtl-Meyer type, the pressure can be found on any tangent line if the pressure and Mach number on the preceding tangent-line element are known. The pressure is taken to be constant on any given tangent-line element. The method is limited as is the method of characteristics to bodies that have supersonic flow behind the nose shock wave. The calculations for this method can be made efficiently using a desk calculator and the tables and charts of reference 12.

In the present investigation, the body contour was approximated by 13 straight-line elements.

Second-Order Shock-Expansion Theory

Second-order shock-expansion theory was developed to provide a closer approximation to the flow field for the cases when $M_\infty\delta_o$ is near 1.0. This was done by developing an approximation to the part of equation (2) that was neglected for the generalized method. Two significant differences from the generalized method arise out of this closer approximation. First, the exact pressure gradient at the nose of the body is found from the method of characteristics. Secondly, along each tangent line used to approximate the body contour, the pressure is found to vary exponentially. The asymptote of the exponential pressure variation is assumed to be equal to the pressure on a cone having the same slope as the tangent-line element and at the same free-stream Mach number.

The application of this method is similar to that of the generalized method except the pressure gradient on each tangent line is found by the relations given in reference 5. The results can be obtained by means of a desk calculator but the process is somewhat tedious.

In the present investigation, the body contour was approximated by 13 straight-line elements.

Tangent-Wedge Method

An approximation to the generalized shock-expansion method is the tangent-wedge method. This approximation is based on the assumption that the pressure on the body at any point is a function of the net flow deflection angle from the free stream. Thus in this method, the pressure at any point on the body can be found from the Rankine-Hugoniot relations for oblique shock waves (for bodies inclined into the free stream) or the Prandtl-Meyer relations (for body surfaces inclined away from the free stream) in which the deflection angle and the upstream Mach number used in these relations are the local angle of the body and the free-stream Mach number, respectively. The method is therefore limited to bodies with angularity less than the detachment angle of a two-dimensional shock wave and could be expected to become accurate in the same regions as the generalized shock-expansion method. The computations for this method are very simple and can be made efficiently by means of a desk calculator and the charts of reference 12.

In the present investigation, the pressure was computed at 14 points along the body.

Impact Theory

A direct approximation to the tangent-wedge method for certain flow fields has resulted in defining an area where Newtonian impact theory becomes applicable. For flows at infinite Mach number, wherein $\gamma = 1.0$ and the shock wave is coincident with the body contour, the expression for the pressure coefficient at any point on the body as given by the tangent-wedge method can be shown to reduce to

$$C_p = 2 \sin^2\delta$$

This expression was obtained by Newton by neglecting centrifugal forces and assuming that the component of the momentum of the free-stream air that is normal to the body surface is absorbed, thereby creating a force on the surface. This theory which is applicable to any body contour would be expected to become applicable for $M_\infty\delta_0 \gg 1.0$. Computations for this theory are very simple and can be made efficiently using a desk calculator.

In the present investigation, the pressure was computed at 14 points along the body.

COMPUTATIONS

Body Contours

Throughout this investigation, a family of profiles whose contours are a function of initial lip angle, δ_o, the diameter ratio d_o/d_m and the fineness ratio l/d_m was used. The equation relating the bodies is given in reference 13 and has the following form:

$$r_b = r_m - (r_m - r_o)(1-x)^{\eta} \tag{8}$$

where η is the relating parameter for the family of curves and is defined by

$$\eta = \frac{\tan \delta_o}{r_m\left(1 - \frac{r_o}{r_m}\right)} \tag{9}$$

The diameter ratio, d_o/d_m, was varied from 0.707 to 0.898. However, for the majority of the investigation, a value of 0.742 was used. This diameter ratio is in the range of values considered in reference 14 and of those necessary to envelop existing turbojet and ramjet engines at about $M_\infty = 3.0$. The diameter ratio was varied while the initial lip angle and fineness ratio were held constant.

The majority of the theoretical investigation was conducted with profiles having a fineness ratio of 5. These profiles are shown in figure 2. A small part of the theoretical investigation was concerned with varying the fineness ratio of the bodies from 0.625 to 10 while the initial lip angle and diameter ratio were held constant.

Wave-Drag Computation

The wave drag was obtained from the following relationship

$$C_D = \int C_p d\left(\frac{A_b}{A_o}\right) \tag{10}$$

The methods discussed previously were used to calculate C_p as a function of A_b/A_o. The above integration was carried out graphically.

RESULTS AND DISCUSSION

Pressure Distributions

The distribution of the external pressure coefficients as computed by the seven theories described earlier is presented in figures 3 through 9, and are in the form of static-pressure coefficient, C_p, as a function of local area ratio, A_b/A_o. These curves were subsequently integrated to obtain the wave-drag coefficients.

Comparison of typical pressure distributions is shown in figure 10. From these curves three general comparisons can be made as to the agreement between the method of characteristics and the various approximate theories. The first point of comparison is the magnitude of the initial pressure rise at the nose of the body. Generalized shock-expansion, second-order shock-expansion, and tangent-wedge theory (omitted from the figures because of its closeness to generalized shock-expansion theory) have the same initial static-pressure coefficient as the method of characteristics since all of these theories use the exact pressure at the nose. First-order perturbation theory and impact theory give lower values of initial static-pressure coefficient than the method of characteristics whereas second-order perturbation theory gives a higher value. The second point of comparison is that only second-order perturbation theory and second-order shock-expansion theory predict an initial pressure gradient which is similar to that predicted by the method of characteristics. It should be mentioned that the initial pressure gradient of the second-order shock-expansion method is inherently identical to that of the method of characteristics. Finally, the predicted variation of static-pressure coefficient downstream of the nose differs for the various theories. For a curved body such as investigated herein, the method of characteristics predicts positive pressure coefficients over most of the body and an overexpansion with resulting negative static-pressure coefficients near the base of the body. Three of the theories, first- and second-order perturbation theories, and second-order shock-expansion theory, compare favorably with the method of characteristics for predicting negative static-pressure coefficients for curved bodies. However, positive pressure coefficients were predicted over the entire body by generalized shock-expansion theory, tangent-wedge theory, and impact theory. To summarize, the results of figure 10 indicate that second-order perturbation theory, and second-order shock-expansion theory provide the best agreement with the method of characteristics for these body shapes and Mach numbers.

The variation of the static-pressure coefficient for bodies of varying fineness ratio (l/d_m of 0.625 to 10), but with constant initial lip angle and diameter ratio, is shown in figure 11 for $M_\infty = 2.5$. These distributions were computed by the generalized shock-expansion theory (fig. 11(a)) and the method of characteristics (fig. 11(b)). Both theories indicate that at a given area ratio (A_b/A_o), a lower static pressure can be obtained with a body of higher fineness ratio. The significance of this will be discussed later.

The effect upon the static-pressure coefficient distributions of varying the diameter ratio, while the initial lip angle, fineness ratio, and M_∞ are held constant, is shown in figure 12. It can be seen that the pressure distributions for the bodies are similar in that at the same proportionate area, the pressure is approximately the same.

WAVE DRAG

The theoretical wave-drag coefficients for the bodies having a fineness ratio of 5 and a diameter ratio of 0.742 at Mach numbers of 2.0, 2.5, 3.0, and 4.0 are presented in figure 13. As indicated, there is a large difference in the results as obtained from the various methods throughout the Mach number range of the investigation. These differences are seen better in figure 14 in which the wave drag computed by the method of characteristics is used as a reference and the error in the wave drag as computed by the six approximate methods is shown. The error is given as a function of the two-dimensional hypersonic similarity parameter, $M_\infty\delta_0$. It can be seen that both generalized shock-expansion theory and tangent-wedge theory overestimate the wave drag while impact theory underestimates the wave drag throughout the entire range of $M_\infty\delta_0$ investigated. The error for each of these methods is sizable for values of $M_\infty\delta_0 < 1.0$ but decreases as $M_\infty\delta_0$ increases. The two perturbation theories have good accuracy at low values of $M_\infty\delta_0$ ($M_\infty\delta_0 = 0.1$ to 0.2) but start becoming inaccurate as $M_\infty\delta_0$ increases. The iteration in second-order perturbation theory is seen to be effective in increasing the range of accuracy over that of the first-order solution. Second-order shock-expansion theory has good accuracy in the range near $M_\infty\delta = 1$ but becomes inaccurate at extremely low values of $M_\infty\delta$. The apparent regions of applicability of the various theories are as would be expected from their assumptions discussed previously. A summary of the wave drags obtained by the method of characteristics is presented in figure 15 in the form of a wave-drag parameter, $C_D\,(0.7M_\infty^2)$, as a function of $M_\infty\delta_0$ (ref. 15). It is seen that the wave drags correlate well with a curve representing the mean of the values at any given $M_\infty\delta_0$.

The effect of varying the fineness ratio, l/d_m, on the wave drag as computed by the method of characteristics and generalized shock-expansion theory is shown in figure 16 for bodies with an initial lip angle of 21.156° and a diameter ratio of 0.742, and at a Mach number of 2.5. As was mentioned earlier, the bodies with higher fineness ratios had a lower static pressure existing at the same area. Thus these bodies would have a lower wave drag. The results as shown indicate that the wave drag of open-nosed bodies of revolution (mass flows of unity) is a function of the fineness ratio and that a fineness ratio of at least 3 is necessary to obtain near minimum wave drag.

The variation in wave drag with changes in diameter ratio is shown in figure 17 for generalized shock-expansion theory and the method of characteristics. The data show that the difference in wave drag as computed by the two theories decreases as the diameter ratio approaches 1, a result that could be expected from the assumptions of generalized shock-expansion theory. The wave drag is also seen to decrease almost linearly as the diameter ratio increases.

Computing Time

The final choice of which theory to use in any given case must be governed by the accuracy desired and the computing time available. The computing time and accuracy of the various theories are shown in the following table.

Theory	Computing time, hr	Accuracy
Method of characteristics	40	Best
First-order perturbation	16	Fair
Second-order perturbation	24	Good
Generalized shock expansion	2	Poor
Second-order shock expansion	8	Good
Tangent wedge	1	Poor
Impact	1	Poor

The computing times given are for one person using a desk calculator. All solutions except the method of characteristics are for 14 points on the body. The computing time given for the method of characteristics is for a solution in which the mesh size was allowed to become large ($c/r = 1.0$). Such a solution will give wave-drag coefficients slightly less than those presented in this study. If greater accuracy is desired (finer mesh size) the computing time for hand computation can be considered to increase in proportion to the square of the ratio of the mesh size for $c/r = 1.0$ divided by the mesh size used ($c/r < 1.0$).

CONCLUDING REMARKS

The wave drag of a family of open-nosed bodies of revolution was computed by six approximate theories and the method of characteristics for a Mach number range of 2.0 to 4.0. Using the results from the method of characteristics as a reference, the investigation showed that the three theories which required the shortest computing time, generalized shock-expansion, tangent-wedge, and impact theories were in general the least accurate. First- and second-order perturbation and second-order shock-expansion theories gave more accurate results, predicting the wave drag to within 10 percent of that from the method of characteristics over much of the ranges of Mach number and body shapes investigated. The range of applicability of the theories was found to vary with the perturbation theories giving good results at $M_\infty\delta_O < 1.0$, second-order shock expansion giving good results near $M_\infty\delta_O$ of 1.0 with the generalized shock-expansion, tangent-wedge, and impact theories starting to give good results at $M_\infty\delta_O \gg 1.0$. In general, considering computing time as well as accuracy, second-order shock-expansion theory was the most attractive within the range of variables investigated herein.

The effect of varying the fineness ratio, l/d_m, on the wave drag was investigated by the use of two theories, the method of characteristics and generalized shock-expansion theory. The results of both theories indicate that for bodies of the type investigated in this study and having the same initial lip angle and diameter ratio, near minimum wave drag can be obtained with a fineness ratio above 3.0.

The wave drag was also computed for bodies having various diameter ratios with the same initial lip angle and fineness ratio. For these bodies, both the method of characteristics and generalized shock-expansion theory predict a near linear decrease in wave drag as the diameter ratio increases.

Ames Aeronautical Laboratory
National Advisory Committee for Aeronautics
Moffett Field, Calif., Aug. 21, 1958

APPENDIX A

NOTATION

For convenience the list of symbols has been divided into two groups, those used throughout the paper and those used exclusively in appendix B. Following are those symbols in the first group.

A	area, sq ft
a	speed of sound, ft/sec
C_D	wave-drag coefficient, $\frac{D}{q_\infty A}$
C_p	static-pressure coefficient, $\frac{p_b - p_\infty}{q_\infty}$
c	distance from point to point along Mach lines in method of characteristics solution divided by l
D	drag, lb
d	body diameter, ft
l	total length of body, ft
M	Mach number
p	static pressure, lb/sq ft
p_t	stagnation pressure, lb/sq ft
q	dynamic pressure, lb/sq ft
r	radial distance divided by l
s	distance along Mach lines in method of characteristics
U	free-stream velocity parallel to x axis
u	axial component of velocity
v	radial component of velocity
x	distance along axis of body from origin divided by l
β	$\sqrt{M^2 - 1}$
γ	ratio of specific heat at constant pressure to specific heat at constant volume

δ stream angle, radians

η parameter relating body shapes (see eq. (9))

θ shock-wave angle, radians

λ $\frac{2\gamma p}{\sin 2\mu}$

μ Mach angle, $\sin^{-1}\frac{1}{M}$, radians

ρ mass density, slugs/cu ft

φ perturbation potential

Subscripts

b body

m maximum geometric characteristic of body

o characteristics of body at origin

p perturbation quantities

∞ free-stream conditions

The following symbols are used exclusively in appendix B which lists the equations used in calculating the wave drag by the method of characteristics.

c_f distance along first family Mach line from computed point to immediately preceding upstream point divided by l

c_s distance along second family Mach line from computed point to immediately preceding upstream point divided by l

n number of the computed point
(The number sequence proceeds from point nearest body to shock wave and from ray to ray in downstream direction (see fig. 1).)

N number of points in input ray (N = 5 in fig. 1)

ϵ a small arbitrary number indicating closeness of approximation in iterative methods

Subscripts

f	characteristics at point whose number is n-1 and which lies on first family Mach line immediately preceding computed point
n	characteristics at point of number n
s	characteristics at point whose number is n+1-N and which lies on second family Mach line immediately preceding computed point
w	characteristics at point whose number is n-N and which lies on shock wave immediately preceding computed point on shock wave
1,2,...i	number of iterations

Superscripts

',",i	iterations

APPENDIX B

CALCULATIONS BY METHOD OF CHARACTERISTICS

Solutions by the method of characteristics presented in this paper were computed by an automatic digital computing machine. The equations used in the solution are also applicable to manual computation. They are therefore listed and discussed herein for ready reference of the interested reader.

In the application of the method of characteristics to the calculation of the static pressure on a body of revolution, the axially symmetric flow field bounded by the body surface and the nose shock wave is subdivided by a network of lines inclined to the local streamline at the local Mach angle (see fig. 1). Points are defined as the intersection of a pair of such lines (field points), the intersection of a line with the body contour (body point), or the intersection of a line with the shock wave (shock-wave point). A ray is defined as the line containing a series of points connected by first family Mach lines. Thus in figure 1, points 1 to 7 and 8 to 14 lie on two separate rays.

Two types of equations are required in the solution, those which define the coordinates of the point and those which define the aerodynamic properties at the point. The calculation of the coordinates and aerodynamic properties proceeds from point to point along a ray, commencing at the body and ending at the shock wave, and then from ray to ray in the downstream direction until the end of the body is reached. In the following discussion, the equations will be grouped according to whether the point is on the input ray, or a field, body, or shock-wave point downstream of the input ray. The equations are given in terms of an arbitrary point so they can be used in the repetitive type of calculation required by the method of characteristics.

Characteristics of Points on Input Ray

The input ray is located on a first family Mach line sufficiently close to the nose of the body that the flow properties at the points can be obtained with the assumption that the shock wave is two-dimensional. In the present case the input ray intersected the body at $x_b \leq 0.001$. The coordinates of points on the input ray are

$$x_n = \frac{N-n}{N-1} x_b + \frac{n-1}{N-1} \left[\frac{r_b - x_b \tan(\mu+\delta) - r_o}{\tan \theta - \tan(\mu+\delta)} \right] \tag{B1}$$

and

$$r_n = \frac{N-n}{N-1} r_b + \frac{n-1}{N-1} \left\{ \frac{[r_b - x_b \tan(\mu+\delta)]\tan\theta - r_o \tan(\mu+\delta)}{\tan\theta - \tan(\mu+\delta)} \right\} \tag{B2}$$

where θ is the two-dimensional shock-wave angle corresponding to a deflection equal to δ_o and μ and δ are the flow characteristics behind the wave.

It should be mentioned that the equations discussed hereinafter are adaptable for determining the entire flow field about a closed-nosed body of revolution as well as the open-nosed bodies studied in this paper. In the former case, the flow behind the nose shock must be supersonic.

Characteristics of Field Points

The equations for the coordinates of the field points are:

$$r_n = \frac{x_o - x_f + r_s \cot(\mu-\delta)_s + r_f \cot(\mu+\delta)_f}{\cot(\mu-\delta)_s + \cot(\mu+\delta)_f} \tag{B3}$$

and

$$x_n = (r_s - r_n)\cot(\mu-\delta)_s + x_s \tag{B4}$$

The distances along the Mach lines from the calculation point to the preceding known points are given by:

$$c_f = \frac{r_n - r_f}{\sin(\mu+\delta)_f} \tag{B5}$$

$$c_s = \frac{r_s - r_n}{\sin(\mu-\delta)_s} \tag{B6}$$

The first and second family compatibility equations, equation (2) in the body of the paper, are put in finite difference form expressing the difference between the aerodynamic properties at point n and the preceding points along the first and second family Mach lines, and are solved simultaneously to give for the stream angle at point n

$$\delta_n = \frac{1}{\lambda_f + \lambda_s} \left[\left(\frac{p}{p_\infty}\right)_f - \left(\frac{p}{p_\infty}\right)_s + (\lambda\delta)_f + (\lambda\delta)_s - \frac{c_f(\lambda \sin\mu \sin\delta)_f}{r_f} + \frac{c_f(\lambda \sin\mu \sin\delta)_s}{r_s} \right] \tag{B7}$$

and the static-pressure ratio

$$\left(\frac{p}{p_\infty}\right)_n = \lambda_o\left[\delta_n-\delta_s - \frac{c_s(\sin\mu \sin\delta)_s}{r_s}\right] \tag{B8}$$

Assuming the total pressure to vary linearly with distance normal to streamline and the variation of stream angle to be small in the vicinity of point n gives

$$\left(\frac{p_t}{p_{t_\infty}}\right)_n = \left(\frac{c_f\sin\mu_f}{c_f\sin\mu_f+c_s\sin\mu_s}\right)\left[\left(\frac{p_t}{p_{t_\infty}}\right)_s-\left(\frac{p_t}{p_{t_\infty}}\right)_f\right]+\left(\frac{p_t}{p_{t_\infty}}\right)_f \tag{B9}$$

The ratio of local static pressure to local total pressure is

$$\left(\frac{p}{p_t}\right)_n = \left(\frac{p}{p_\infty}\right)_n\left(\frac{p_{t_\infty}}{p_t}\right)_n\left(\frac{p_\infty}{p_{t_\infty}}\right) \tag{B10}$$

from which

$$M_n = \sqrt{\frac{2}{\gamma-1}\left[\left(\frac{p}{p_t}\right)_n^{\frac{1-\gamma}{\gamma}}-1\right]} \tag{B11}$$

and hence

$$\mu_n = \sin^{-1}\frac{1}{M_n} \tag{B12}$$

Characteristics of Body Points

The body point n is at the intersection of the second family Mach line from point n + 1 - N and the body contour. Hence the coordinate equations are dependent on the analytic expression for the body contour. If the expression is not simple, an explicit solution of the intersection point may be impossible, as in the present case. In such cases Newton's approximation can be used to solve for the axial location of the point as follows. Let the difference between the body radius and the radial distance of the second family Mach line from point n + 1 - N at the same value of x be expressed as

$$f(x) = r_b(x)-r_s+(x-x_s)\tan(\mu-\delta)_s \tag{B13}$$

where $r_b(x)$ is the analytic expression for the body contour, so that at point of intersection

$$f(x_n) = 0 \tag{B14}$$

To solve for x_n, let $x \equiv x_1 = x_s$ and solve

$$x_2 = x - \frac{f(x)}{df(x)/dx} = x_1 - \frac{f(x_1)}{df(x_1)/dx} \tag{B15}$$

Repeat this operation letting $x \equiv x_2$ and continue until

$$x_i - x_{i-1} < \epsilon \tag{B16}$$

The value of x_n is taken to be x_i. Then the radius at the intersection point is

$$r_n = r_s - (x_n - x_s)\tan(\mu - \delta)_s \tag{B17}$$

The distance along the second family Mach line from point n to the preceding point, c_s, is given by equation (B6) and the stream angle, δ_n, is given by the slope of the body contour. These two values are used in equation (B8) to determine the static pressure on the body at point n. The static-pressure coefficient is then given by

$$C_p = \frac{(p/p_\infty)_n - 1}{(\gamma/2)M_\infty^2} \tag{B18}$$

Since the body contour is a streamline, the total pressure remains constant along the body. The remaining flow characteristics are determined from equations (B10) to (B12).

Characteristics of Shock-Wave Point

The shock-wave point, n, is at the intersection of the first family Mach line from point n-1 and the shock wave from point n-N. The coordinates are given by

$$x_n = \frac{x_w \tan \theta_w - x_f \tan(\mu+\delta)_f + r_f - r_w}{\tan \theta_w - \tan(\mu+\delta)_f} \tag{B19}$$

and

$$r_n = (x_n - x_f)\tan(\mu+\delta)_f + r_f \tag{B20}$$

The distance along the first family Mach line, c_f, is given by equation (B5).

A simple explicit relation involving the static pressure and deflection angle immediately behind a shock wave is not available. It is therefore impractical, and probably impossible, to determine the static

pressure and deflection angle at the shock-wave point by solving simultaneously the equation relating pressure and deflection angle across the shock and the one compatibility equation available. Iterative methods are therefore used. The compatibility equation available is

$$\delta_n = \frac{\left(\frac{p}{p_\infty}\right)_f - \left(\frac{p}{p_\infty}\right)_n}{\lambda_f} + \delta_f - \frac{c_f(\sin \mu \sin \delta)_f}{r_f} \tag{B21}$$

To commence the iterative procedure, let

$$\left(\frac{p}{p_\infty}\right)_n \equiv \left(\frac{p}{p_\infty}\right)_n' = \left(\frac{p}{p_\infty}\right)_f \tag{B22}$$

and find δ_n' from equation (B21). The stream angle δ_n' is taken as the deflection angle for a two-dimensional shock wave at point n and the shock-wave angle computed from

$$\sin^6\theta_n' + g \sin^4\theta_n' + h \sin^2\theta_n' + j = 0 \tag{B23}$$

where

$$\left.\begin{aligned} g &= -\frac{M_\infty^2+2}{M_\infty^2} - \gamma \sin^2\delta_n' \\ h &= \frac{2M_\infty^2+1}{M_\infty^4} + \left[\frac{(\gamma+1)^2}{4} + \frac{(\gamma-1)}{M_\infty^2}\right]\sin^2\delta_n' \\ j &= -\frac{\cos^2\delta_n'}{M_\infty^4} \end{aligned}\right\} \tag{B24}$$

Equation (B23) is solved most readily by Newton's approximation. Briefly let

$$f(\theta') = \sin^6\theta' + g \sin^4\theta' + h \sin^2\theta' + j \tag{B25}$$

so that at point n

$$f(\theta') \equiv f(\theta_n') = 0 \tag{B26}$$

To solve for θ_n', let $\theta' \equiv \theta_1' = \theta_w$ and solve

$$\sin^2\theta_2' = \sin^2\theta' - \frac{f(\theta')}{df(\theta')/d \sin^2\theta'} = \sin^2\theta_1' - \frac{f(\theta_1')}{df(\theta_1')/d \sin \theta_1'} \tag{B27}$$

Repeat the operation letting $\theta' = \theta_2'$ and continue until

$$\theta_i' - \theta_{i-1}' < \epsilon \tag{B28}$$

The value of θ_n' is taken to be θ_i'.

The static-pressure ratio across a shock wave corresponding to a given shock-wave angle is

$$\frac{p}{p_\infty} = \frac{2\gamma M_\infty^2 \sin^2\theta - (\gamma-1)}{\gamma+1} \tag{B29}$$

The static pressure at point n is then taken as

$$\left(\frac{p}{p_\infty}\right)_n'' = \frac{1}{2}\left[\left(\frac{p}{p_\infty}\right)_n' + \frac{2\gamma M_\infty^2 \sin^2\theta - (\gamma-1)}{\gamma+1}\right] \tag{B30}$$

Let

$$\left(\frac{p}{p_\infty}\right)_n \equiv \left(\frac{p}{p_\infty}\right)_n'' \tag{B31}$$

in equation (B21) and solve for δ_n''. The process involving equations (B23) to (B31) is repeated until

$$\delta_n^{\,i} - \delta_n^{\,i-1} < \epsilon \tag{B32}$$

Then

$$\left.\begin{aligned}\left(\frac{p}{p_\infty}\right)_n &= \left(\frac{p}{p_\infty}\right)_n^{\,i} \\ \delta_n &= \delta_n^{\,i}\end{aligned}\right\} \tag{B33}$$

The total pressure loss through the shock wave is given by

$$\left(\frac{p_t}{p_{t_\infty}}\right)_n = \left[\frac{(\gamma+1)M_\infty^2 \sin^2\theta_n}{(\gamma-1)M_\infty^2 \sin^2\theta_n + 2}\right]^{\frac{\gamma}{\gamma-1}} \left(\frac{p}{p_\infty}\right)^{\frac{1}{1-\gamma}} \tag{B34}$$

The remainder of the aerodynamic characteristics are found by means of equations (B10) to (B12).

Mesh Size

Accurate solutions of the method of characteristics require that the distance between points, mesh size, be small. However, when the mesh size, c/r, becomes large, it is necessary to iterate the points affected. This iteration consists of averaging the aerodynamic properties of the known and computed points, assigning them to the coordinates of the known point and recomputing the computed point. In the actual machine computation, a c/r of 0.25 was used as the criterion for iteration when N = 10 and 0.10 when N = 20, and the iteration was performed only once.

The computing time (on an IBM 653) for 10 and 20 point solutions was 3/4 and 3 hours, respectively. For curved bodies, the difference in static-pressure coefficient distribution from 10 and 20 point solutions was insignificant. For straight bodies, however, it was found necessary to start at $x < 0.001$ in order to obtain a pressure distribution with no discontinuities.

REFERENCES

1. Brown, Clinton E., and Parker, Hermon M: A Method for the Calculation of External Lift, Moment and Pressure Drag of Slender Open-Nose Bodies of Revolution at Supersonic Speeds. NACA Rep. 808, 1945. (Supersedes NACA WR L-720)

2. Van Dyke, Milton D.: A Study of Second-Order Supersonic-Flow Theory. NACA Rep. 1081, 1952. (Supersedes NACA TN 2200)

3. Liepmann, H. W., and Roshko, A.: Elements of Gasdynamics. John Wiley and Sons, Inc., 1957.

4. Eggers, A. J., Jr., Savin, Raymond C., and Syvertson, Clarence A.: The Generalized Shock-Expansion Method and Its Application to Bodies Traveling at High Supersonic Airspeeds. Jour. Aero. Sci., vol. 22, no. 4, April 1955, pp. 231-238. (Issued as IAS Preprint 487, 1954)

5. Syvertson, Clarence A., and Dennis, David H.: A Second-Order Shock-Expansion Method Applicable to Bodies of Revolution Near Zero Lift. NACA Rep. 1328, 1957. (Supersedes NACA TN 3527)

6. Lees, Lester: Hypersonic Flow. IAS Preprint No. 554, 1955.

7. Newton, Isaac: Principia. Motte's Translation Revised. University of California Press, 1946.

8. Ferri, Antonio: Application of the Method of Characteristics to Supersonic Rotational Flow. NACA Rep. 841, 1946.

9. Liepmann, H. W., and Lapin, Ellis: Summary of Characteristics Methods for Steady State Supersonic Flows. Rep. No. SM-13343, Douglas Aircraft Co., Inc., March 3, 1949.

10. Isenberg, J. S.: The Method of Characteristics in Compressible Flow. Part I. TR No. F-TR-1173A-ND, Air Materiel Command, U. S. Air Force, Dec. 1947.

11. Van Dyke, Milton D.: Practical Calculation of Second-Order Supersonic Flow Past Nonlifting Bodies of Revolution. NACA TN 2744, 1952.

12. Ames Research Staff: Equations, Tables, and Charts for Compressible Flow. NACA Rep. 1135, 1953.

13. Willis, J. H., and Randall, D. G.: The Theoretical Wave Drag of Open-Nose Axisymmetrical Forebodies with Varying Fineness Ratio, Area Ratio, and Nose Angle. RAE TN 2360, British Ministry of Supply, London, 1956. (Also British A.R.C. CP 245, and A.R.C. Rep. 17,694)

14. Evans, Philip J., Jr.: Analytical Investigation of Ram-Jet-Engine Performance in Flight Mach Number Range From 3 to 7. NACA RM E51H02, 1951.

15. Ehret, Dorris M., Rossow, Vernon J., and Stevens, Victor I.: An Analysis of the Applicability of the Hypersonic Similarity Law to the Study of Flow About Bodies of Revolution at Zero Angle of Attack. NACA TN 2250, 1950.

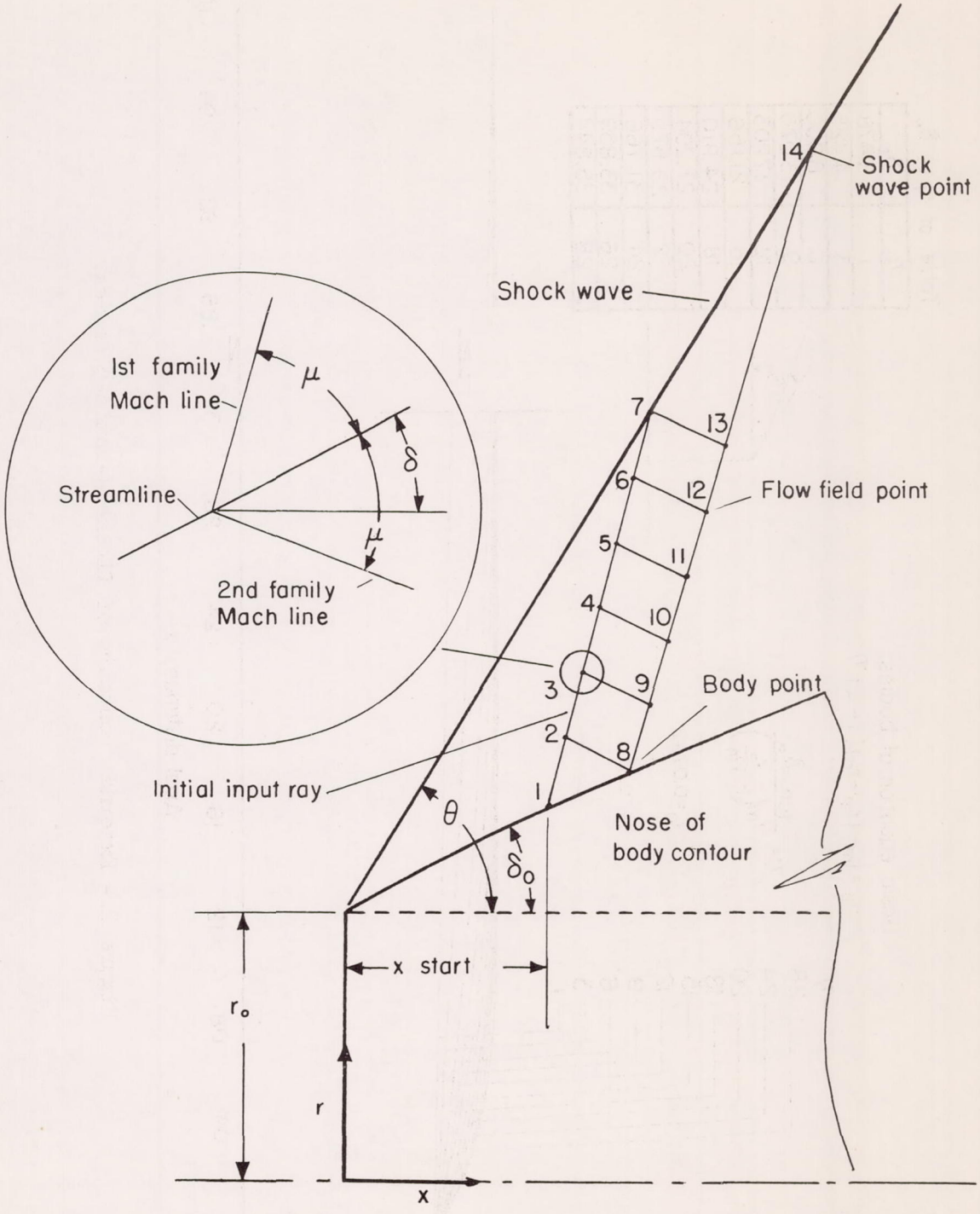

Figure 1.- Schematic diagram of method of characteristics solution.

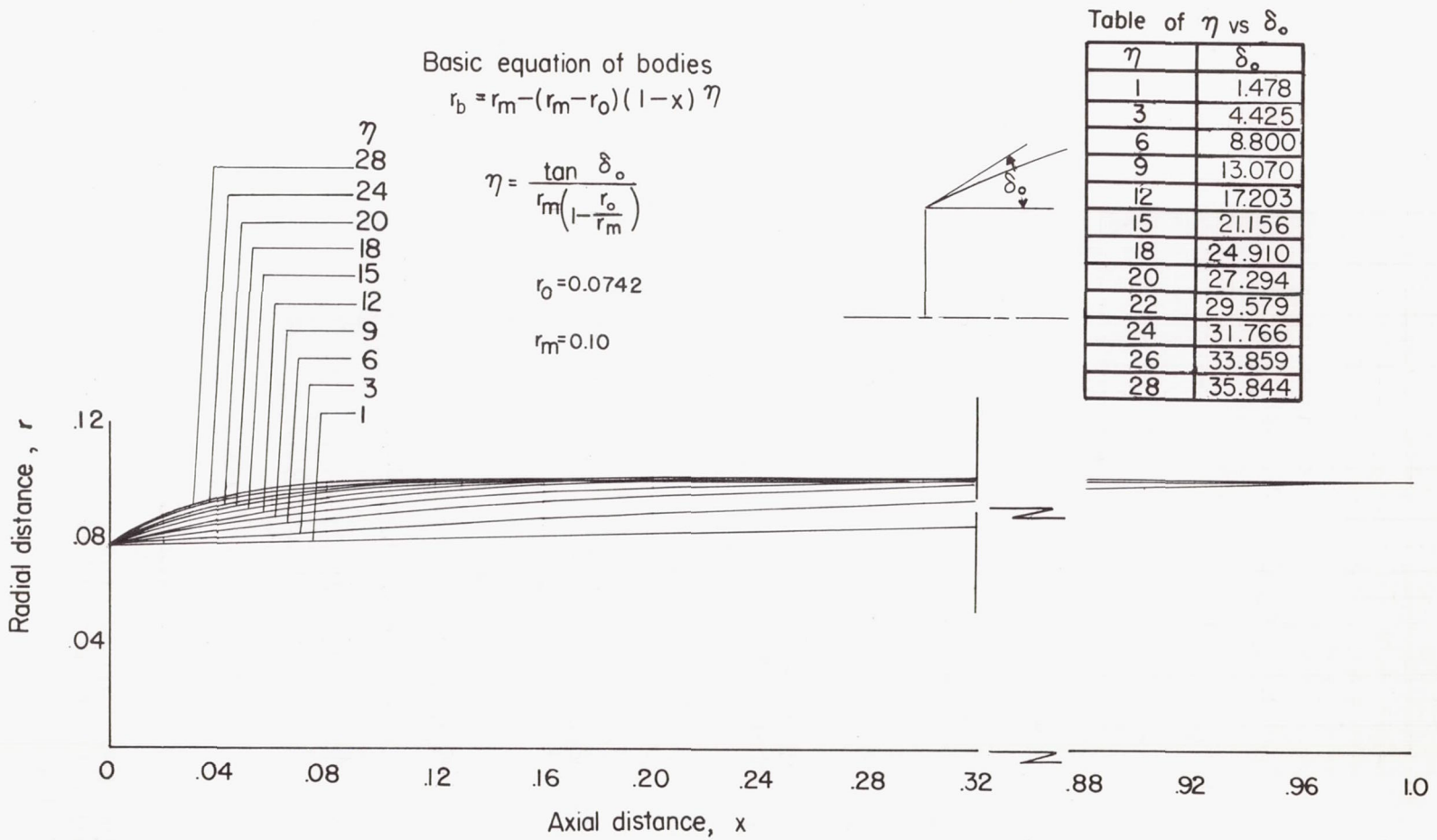

Figure 2.- External contours of fineness-ratio-5 bodies.

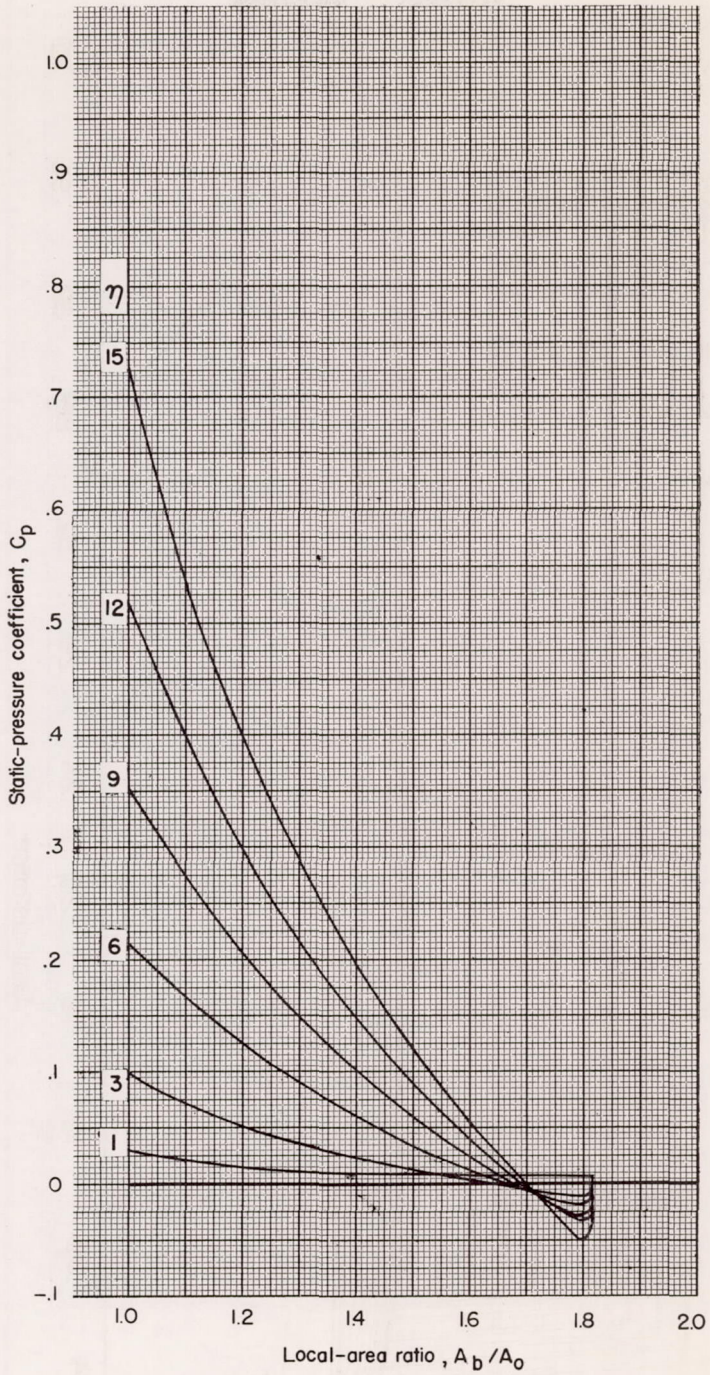

(a) $M_\infty = 2.0$

Figure 3.- The variation of static-pressure coefficient with local-area ratio; method of characteristics; fineness ratio = 5.0; diameter ratio = 0.742.

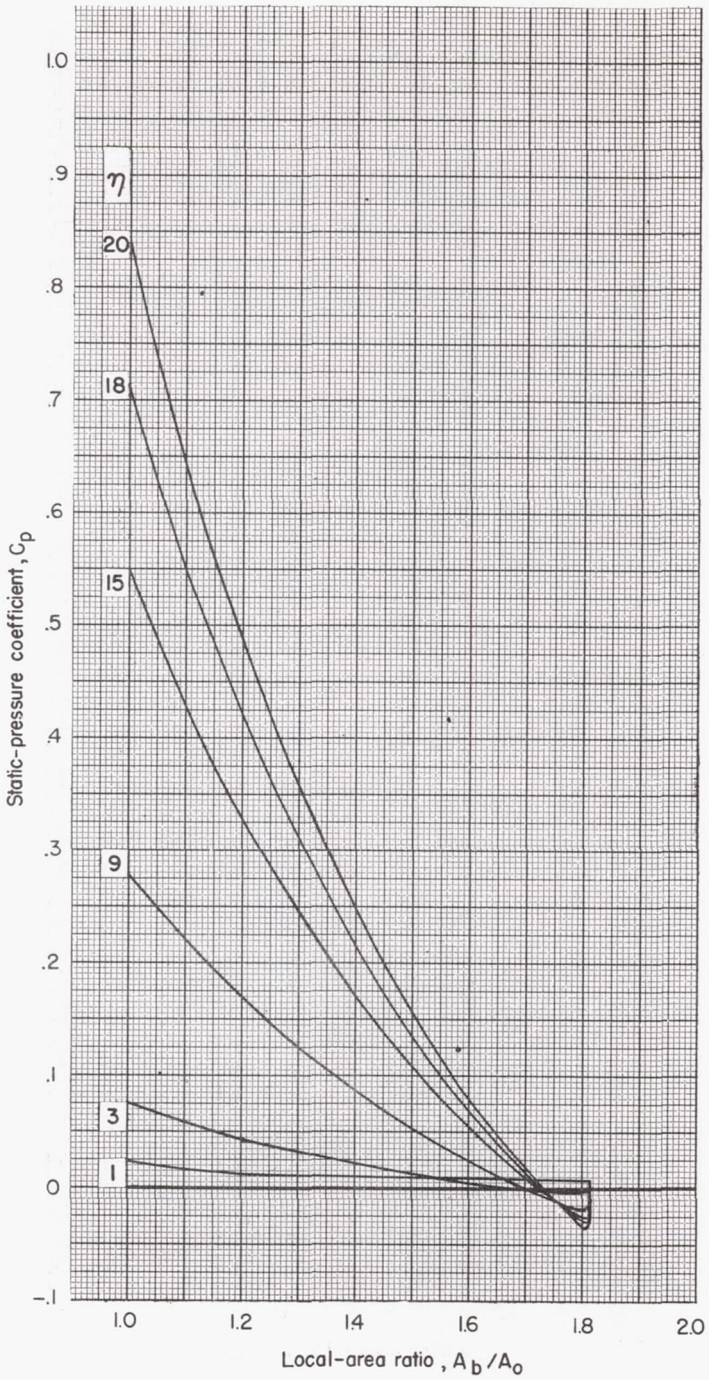

(b) $M_\infty = 2.5$

Figure 3.- Continued.

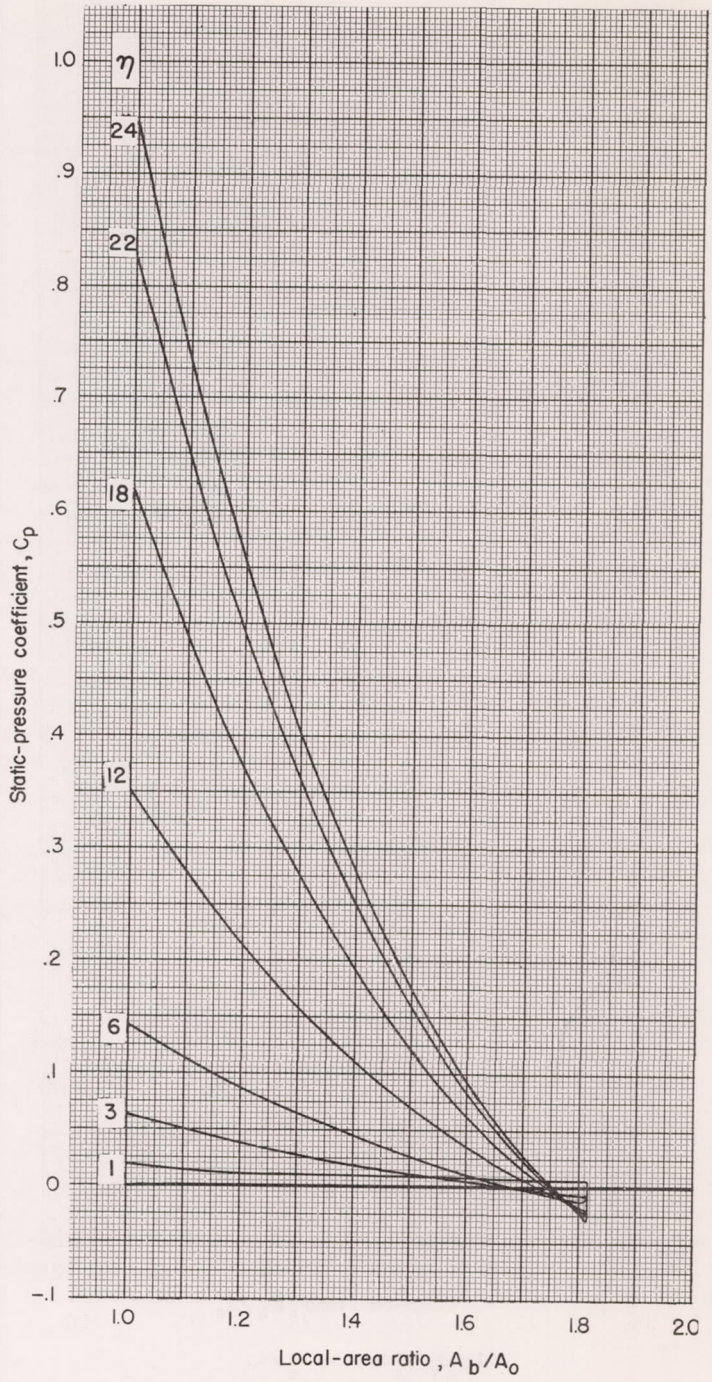

(c) $M_\infty = 3.0$

Figure 3.- Continued.

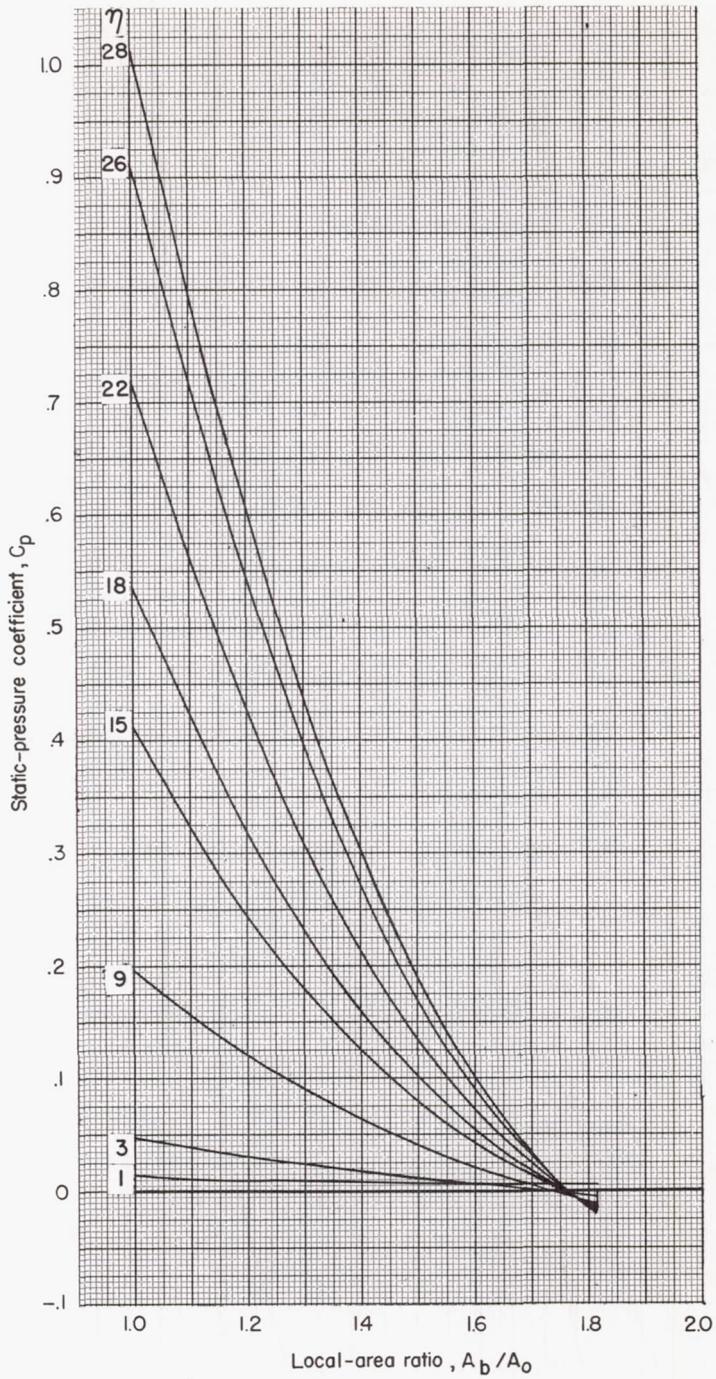

(d) $M_\infty = 4.0$

Figure 3.- Concluded.

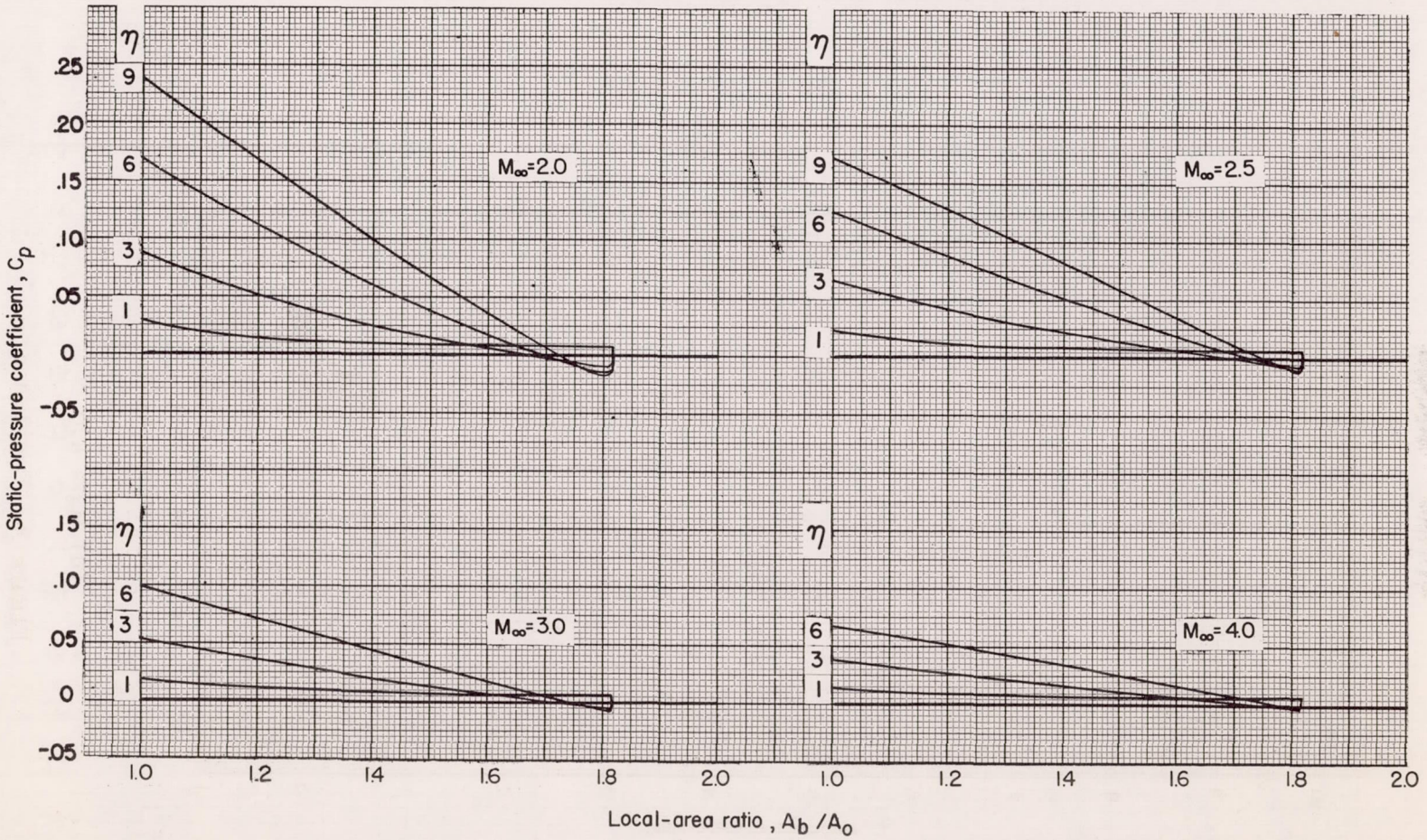

Figure 4.- The variation of static-pressure coefficient with local-area ratio; first-order perturbation theory; fineness ratio = 5.0; diameter ratio = 0.742.

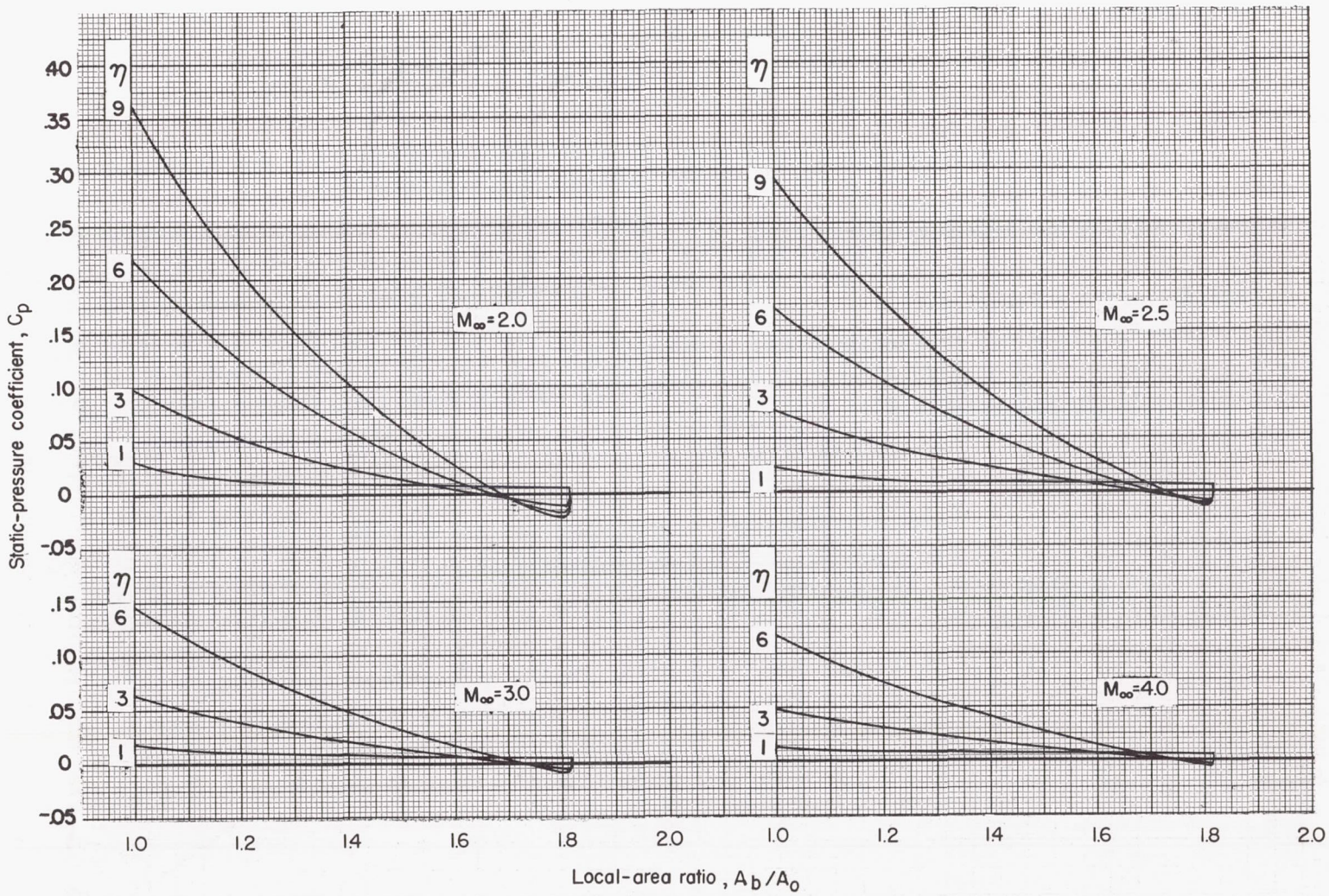

Figure 5.- The variation of static-pressure coefficient with local-area ratio; second-order perturbation theory; fineness ratio = 5.0; diameter ratio = 0.742.

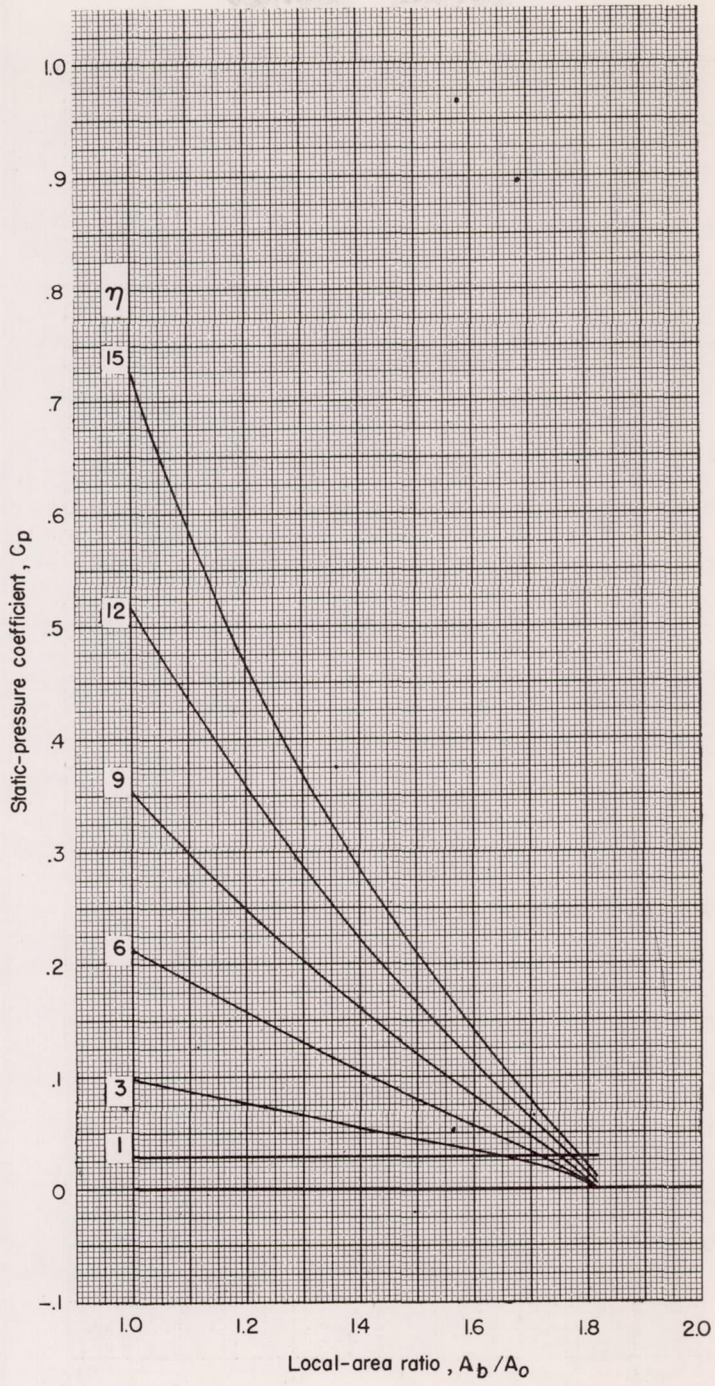

(a) $M_\infty = 2.0$

Figure 6.- The variation of static-pressure coefficient with local-area ratio; generalized shock-expansion theory; fineness ratio = 5.0; diameter ratio = 0.742.

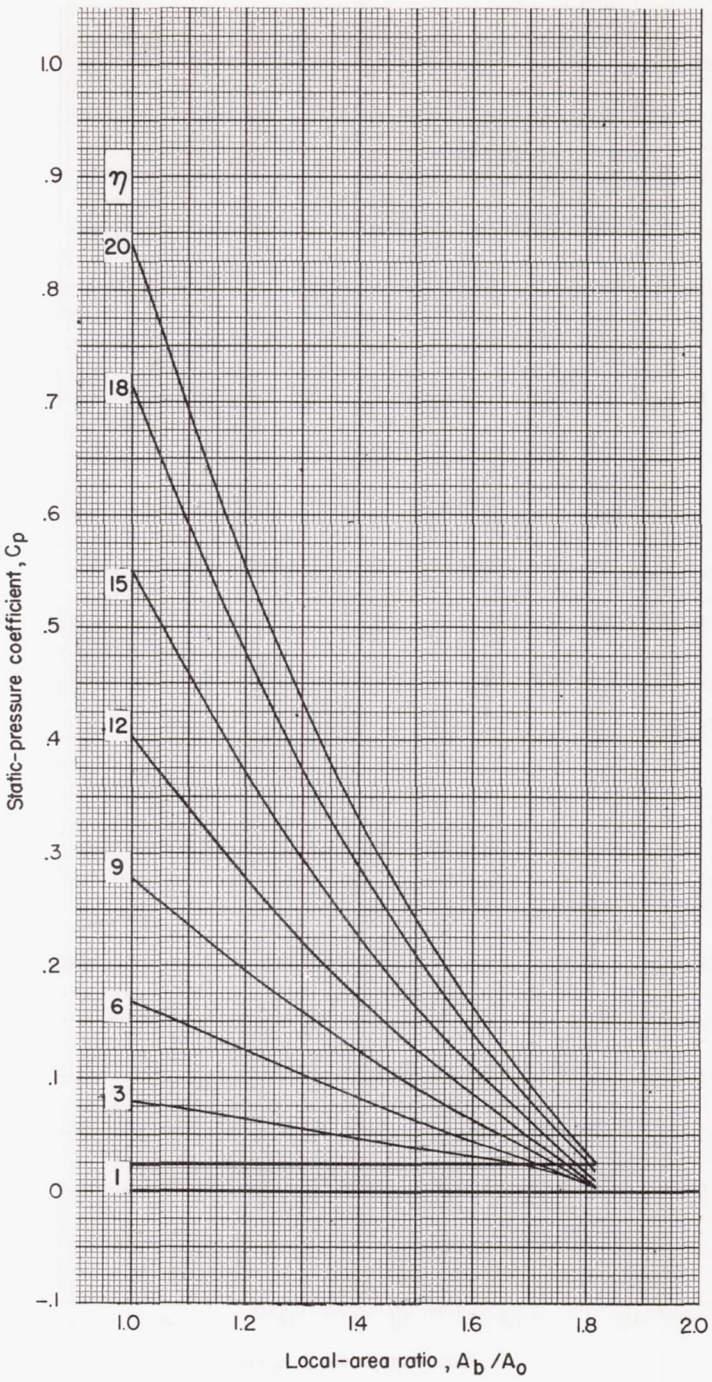

(b) $M_\infty = 2.5$

Figure 6.- Continued.

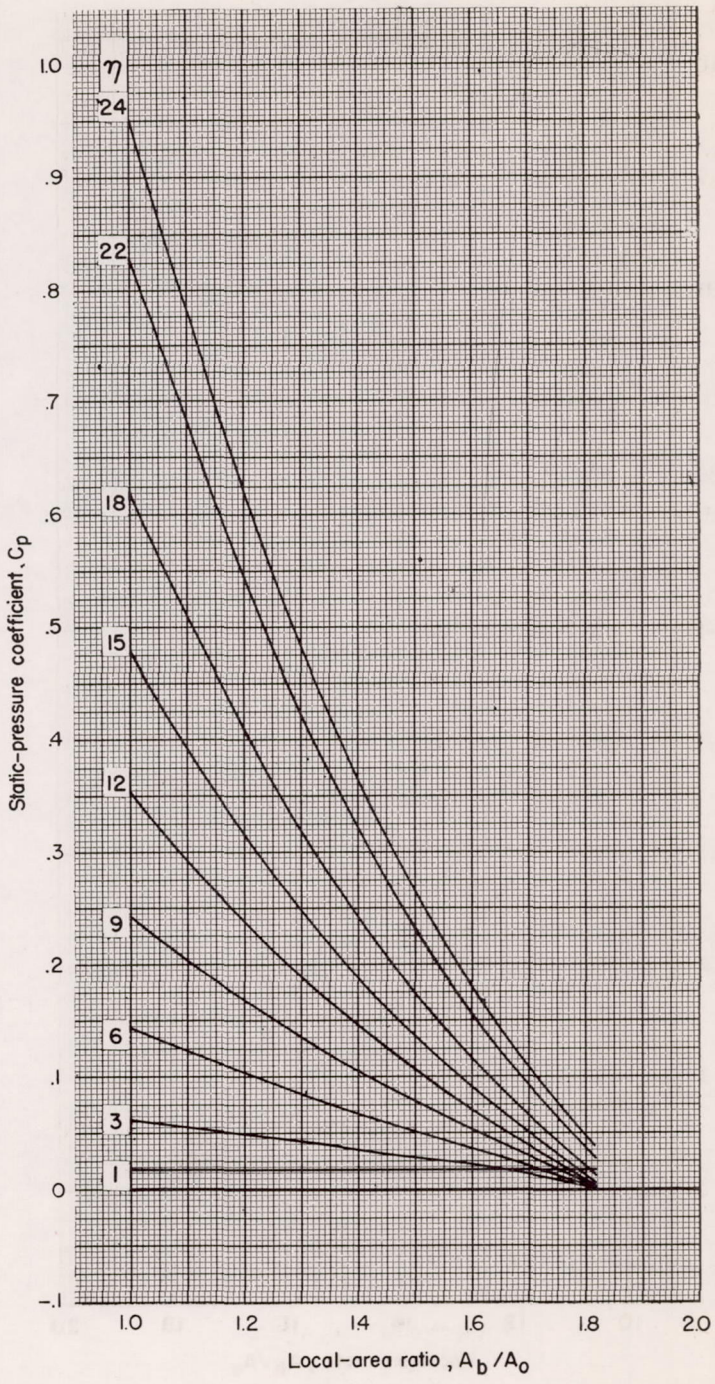

(c) $M_\infty = 3.0$

Figure 6.- Continued.

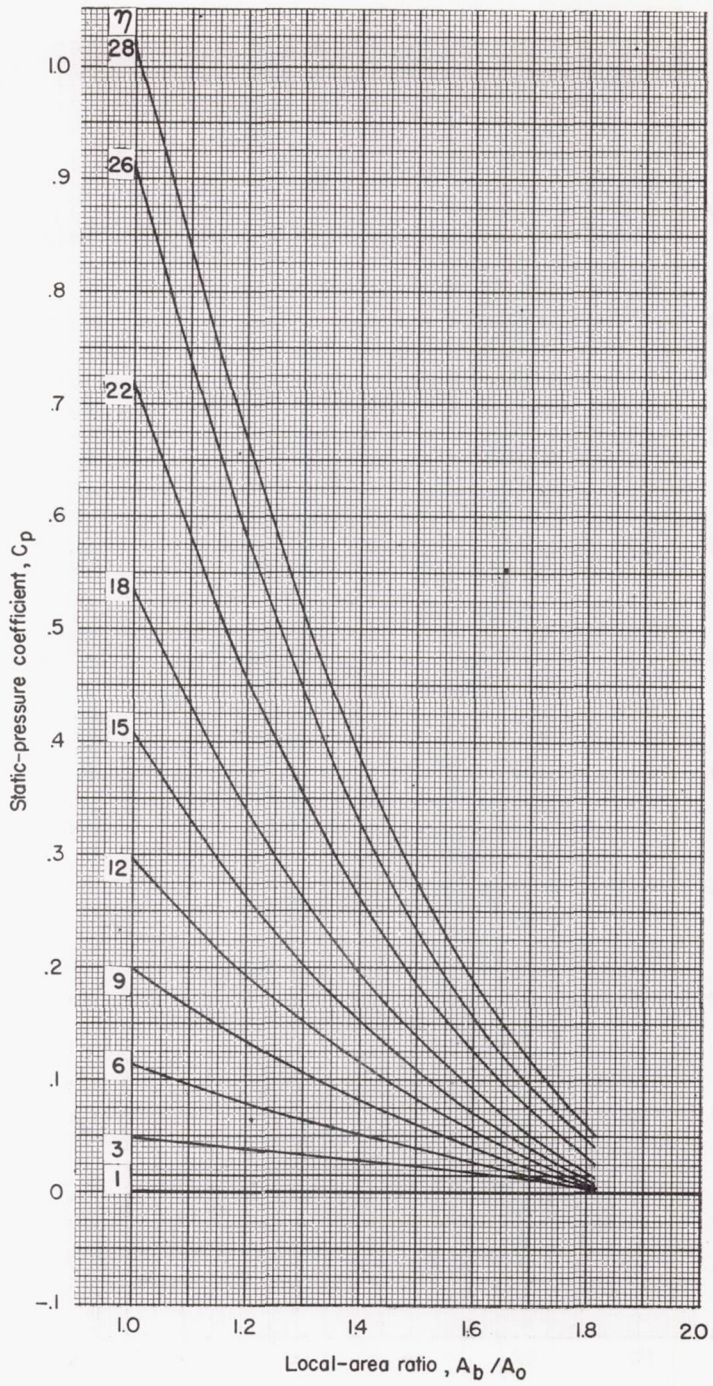

(d) $M_\infty = 4.0$

Figure 6.- Concluded.

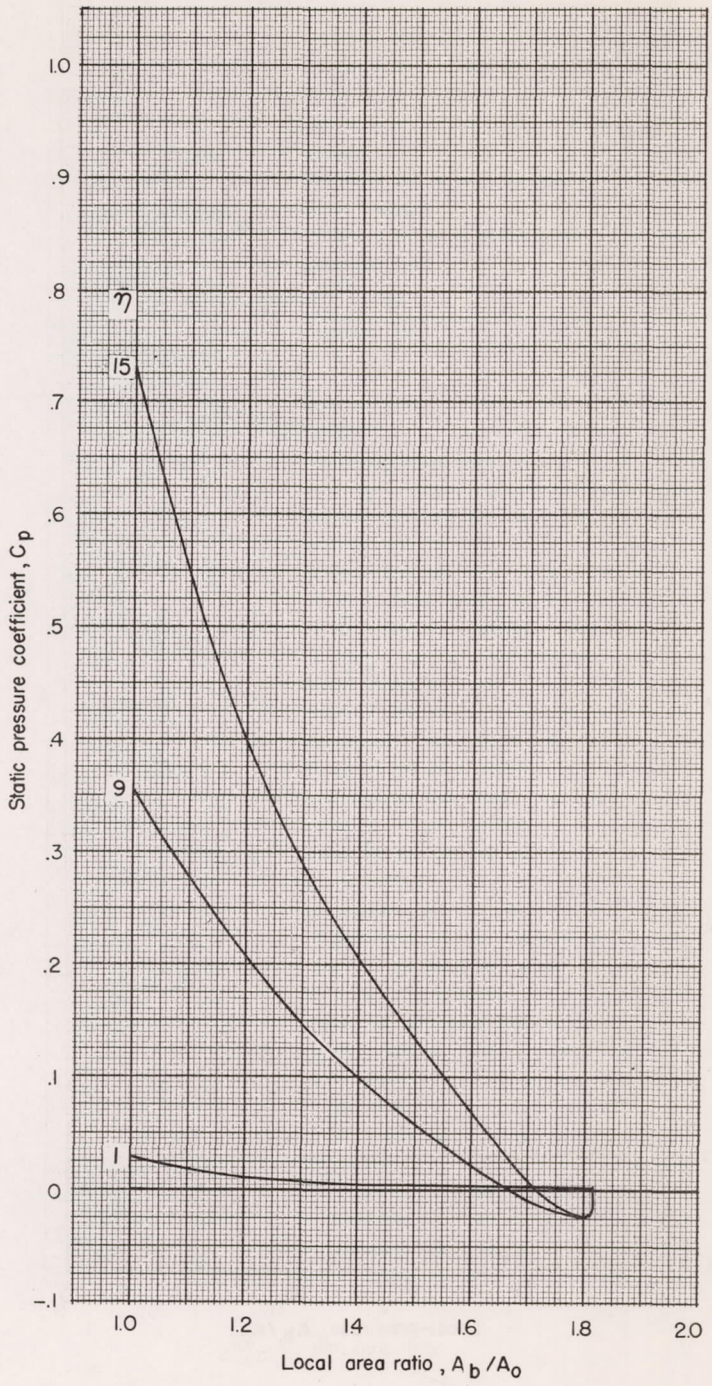

(a) M = 2.0

Figure 7.- The variation of static-pressure coefficient with local-area ratio; second-order shock-expansion theory; fineness ratio = 5.0; diameter ratio = 0.742.

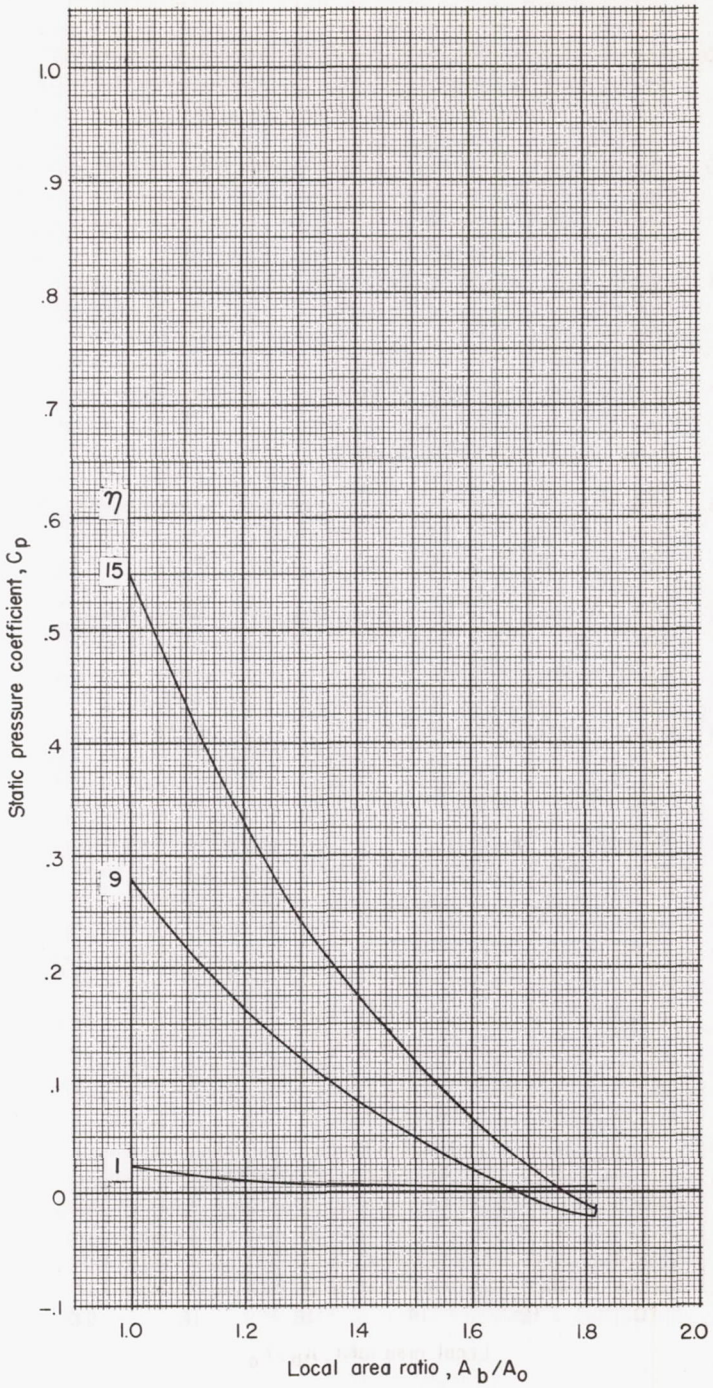

(b) M = 2.5

Figure 7.- Continued.

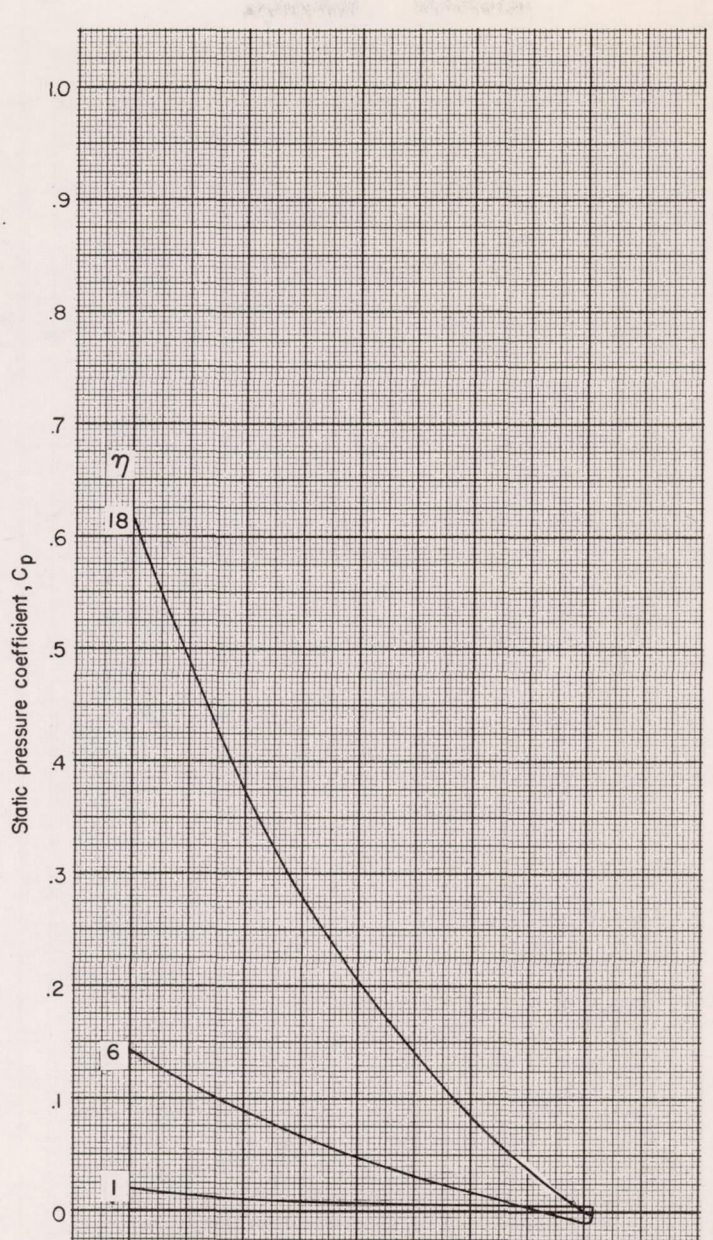

(c) M = 3.0

Figure 7.- Continued.

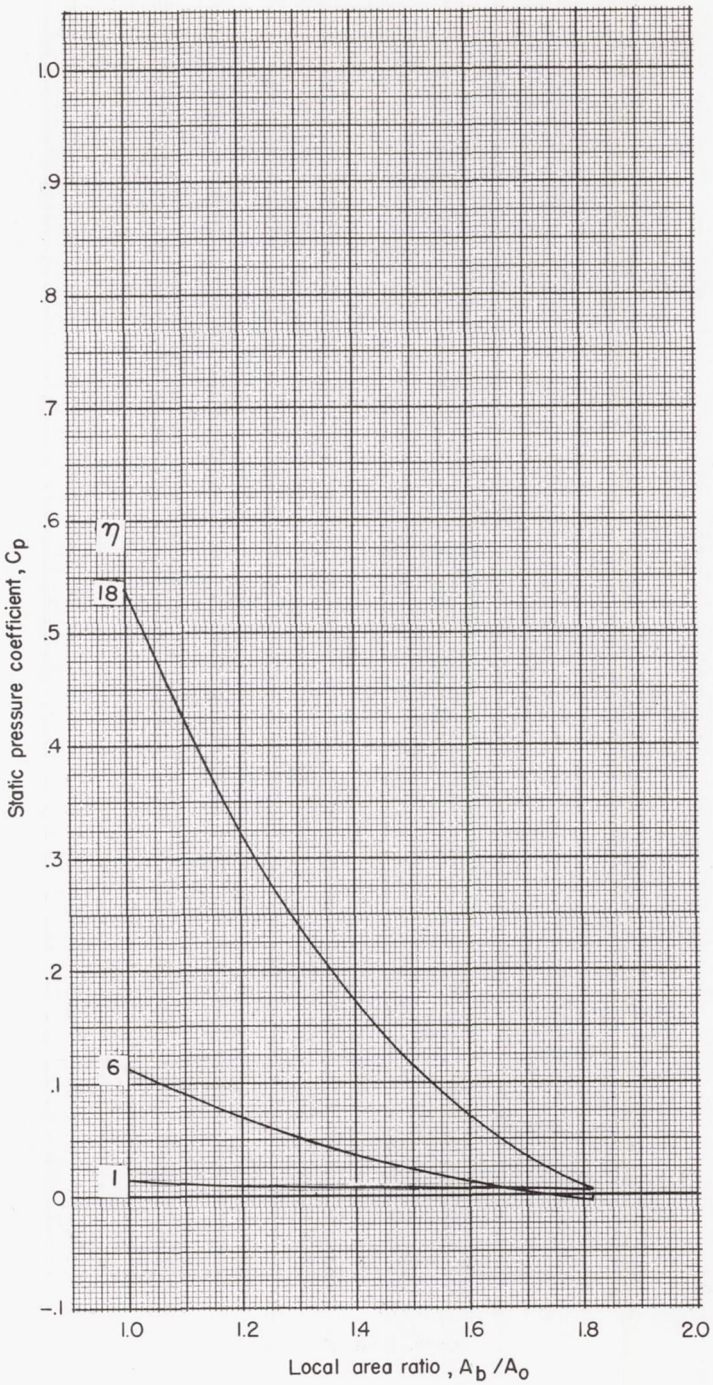

(d) M = 4.0

Figure 7.- Concluded.

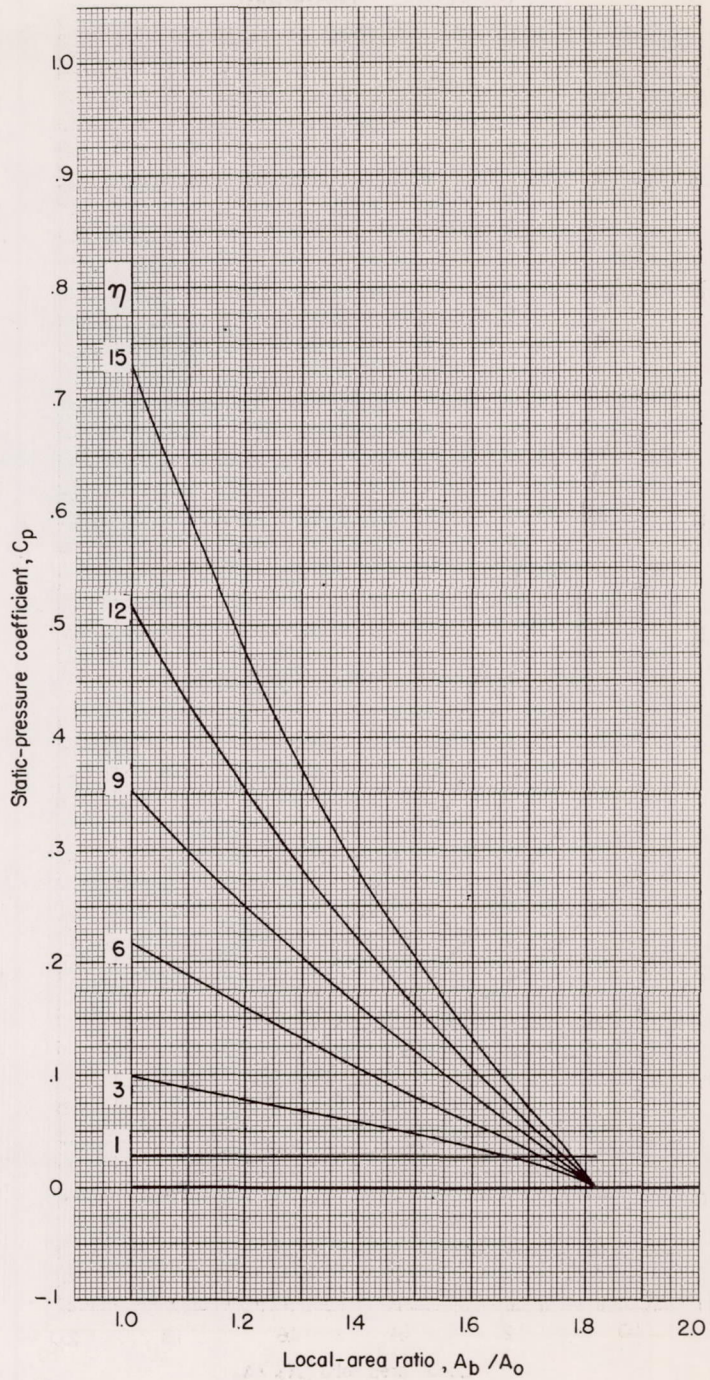

(a) $M_\infty = 2.0$

Figure 8.- The variation of static-pressure coefficient with local-area ratio; tangent-wedge theory; fineness ratio = 5.0; diameter ratio = 0.742.

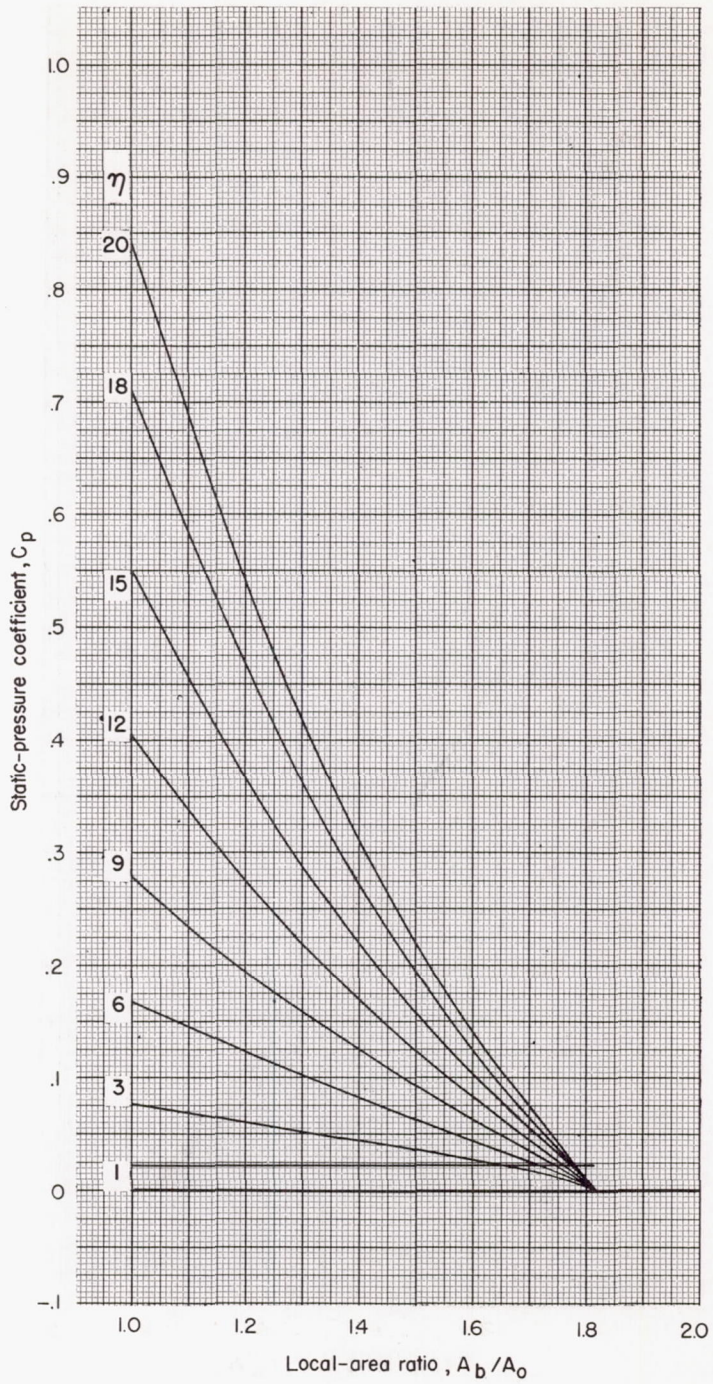

(b) $M_\infty = 2.5$

Figure 8.- Continued.

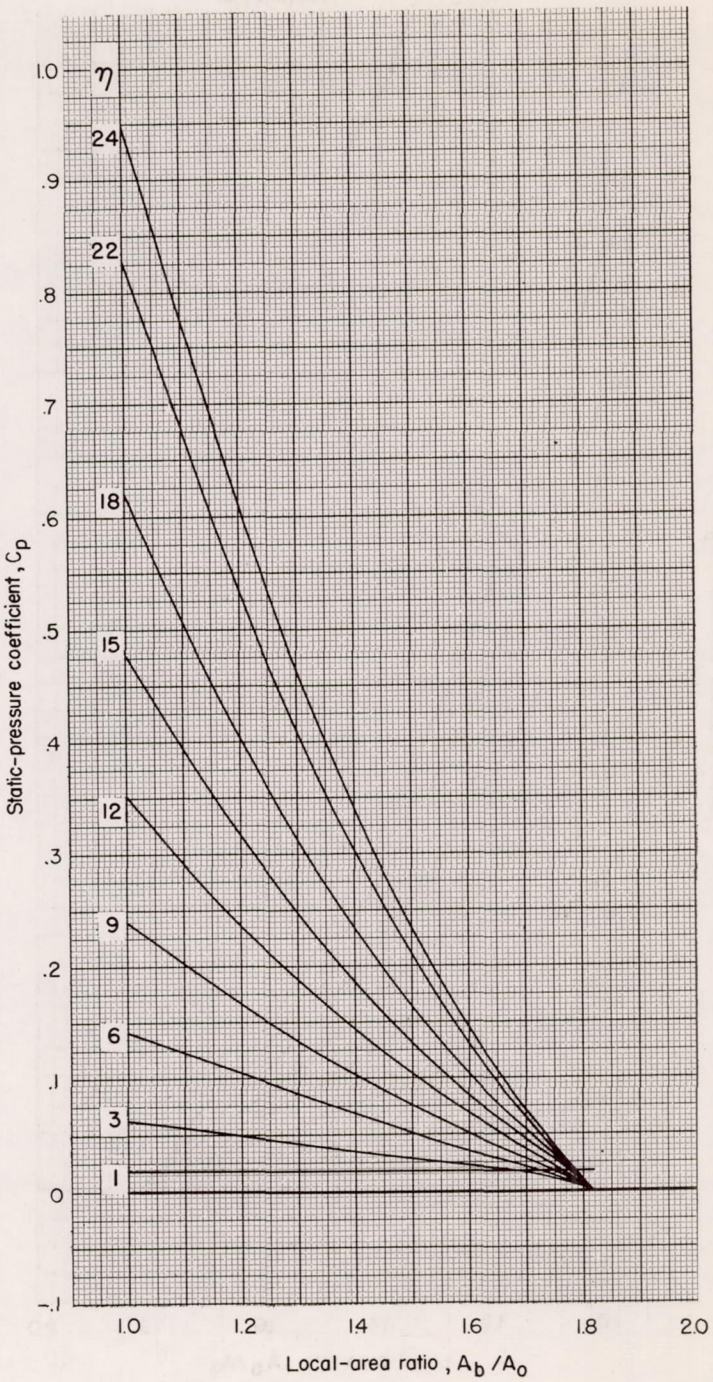

(c) $M_\infty = 3.0$

Figure 8.- Continued.

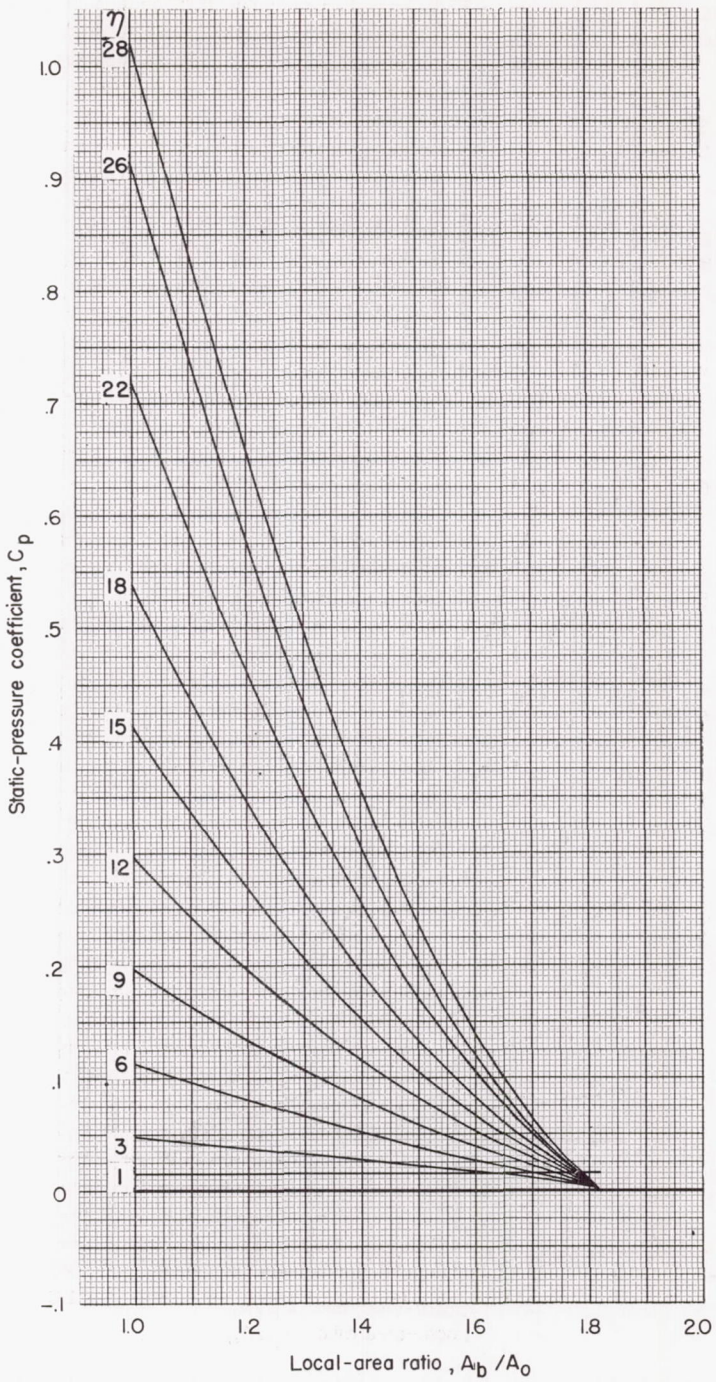

(d) $M_\infty = 4.0$

Figure 8.- Concluded.

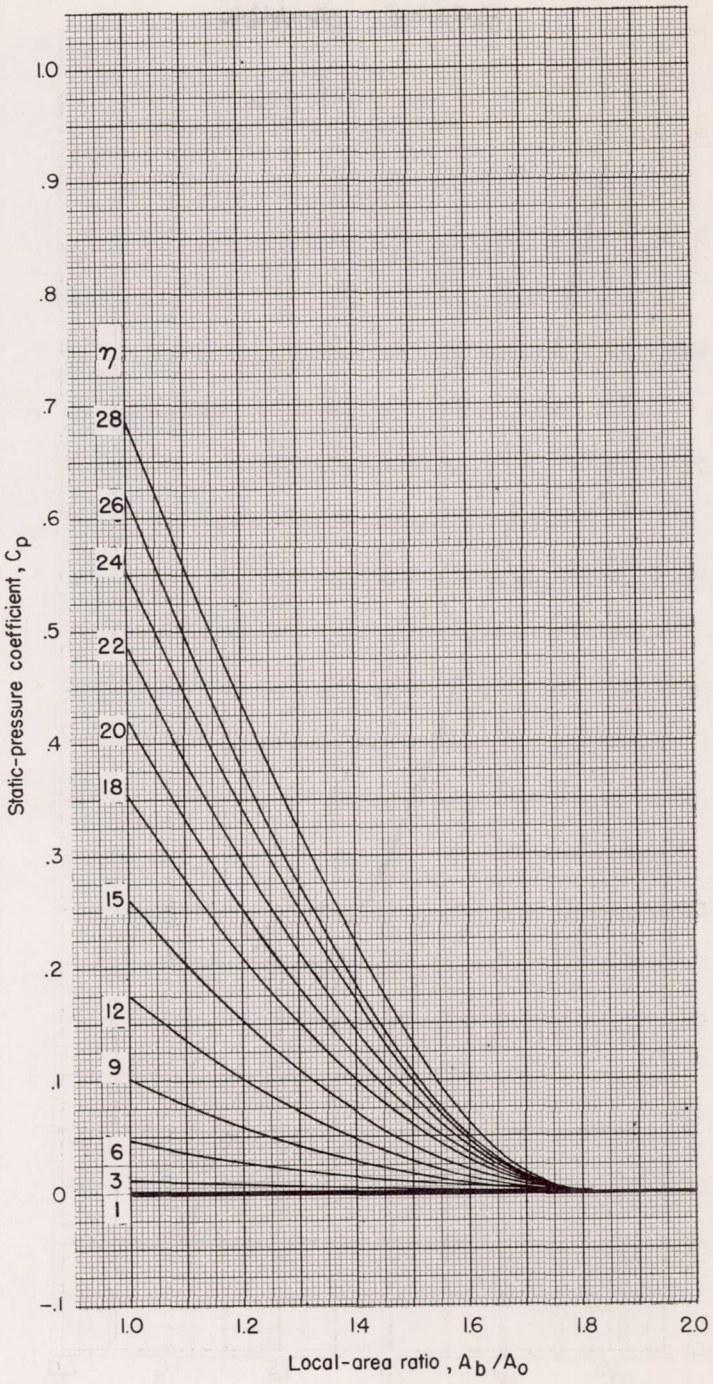

Figure 9.- The variation of static-pressure coefficient with local-area ratio; impact theory; fineness ratio = 5.0; diameter ratio = 0.742.

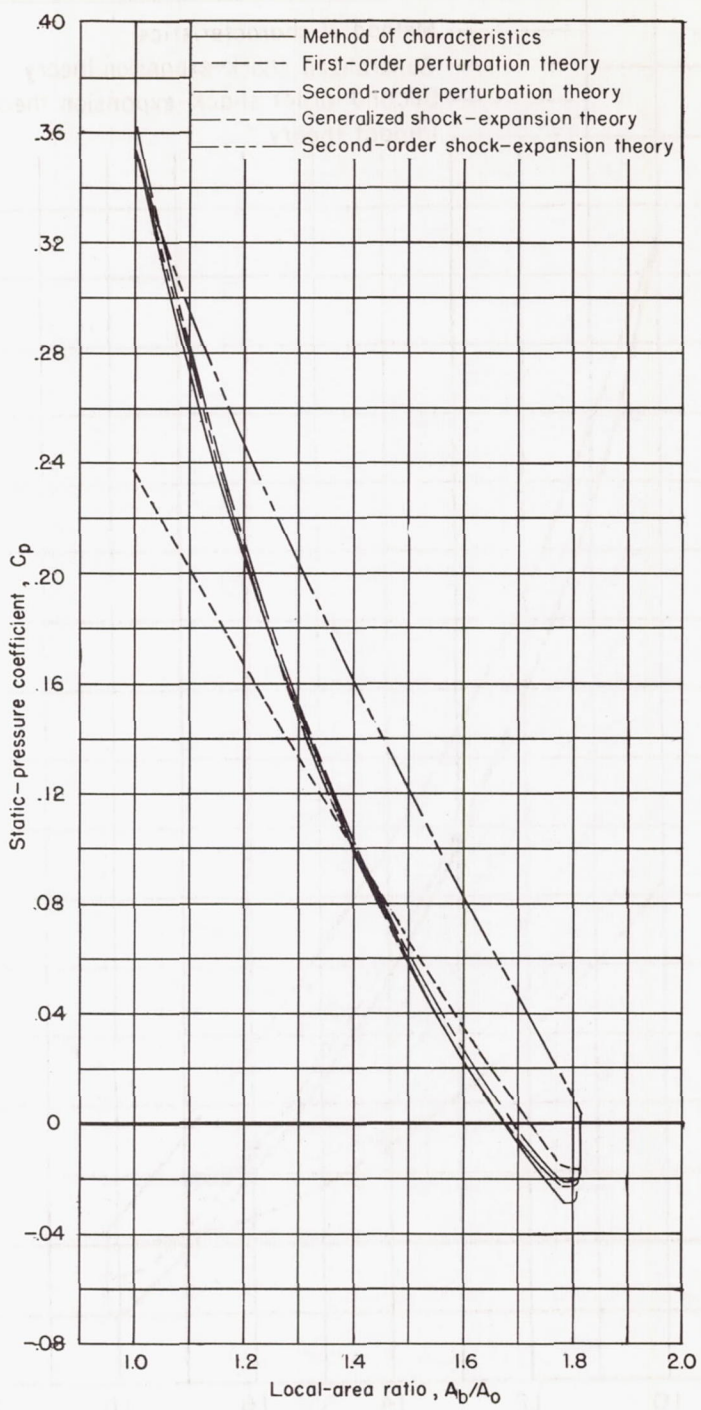

(a) $M_\infty = 2.0$, $\eta = 9$

Figure 10.- Comparisons of typical static-pressure-coefficient distributions for bodies having a fineness ratio of 5.0 and a diameter ratio of 0.742.

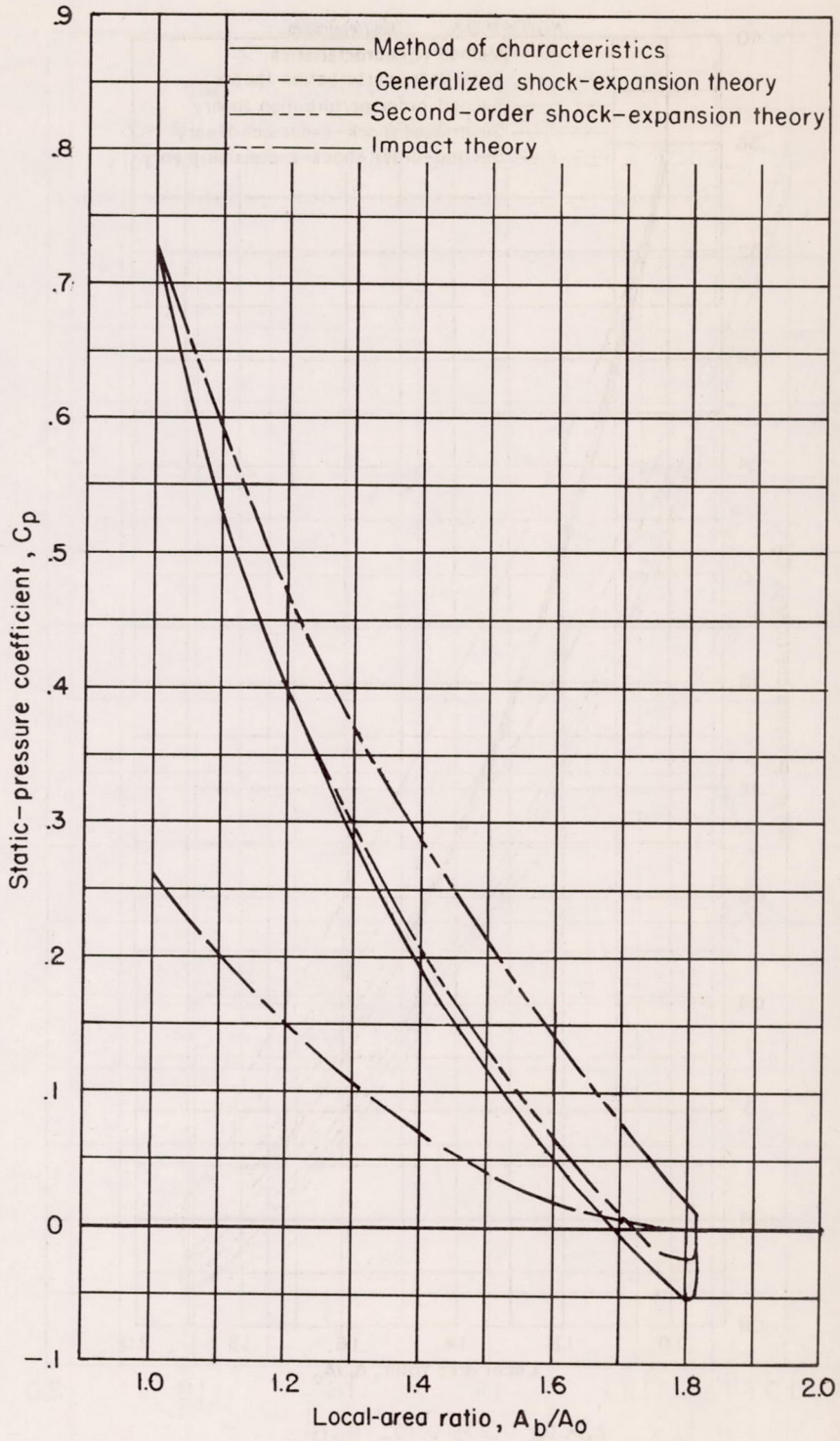

(b) $M_\infty = 2.0$, $\eta = 15$

Figure 10.- Continued.

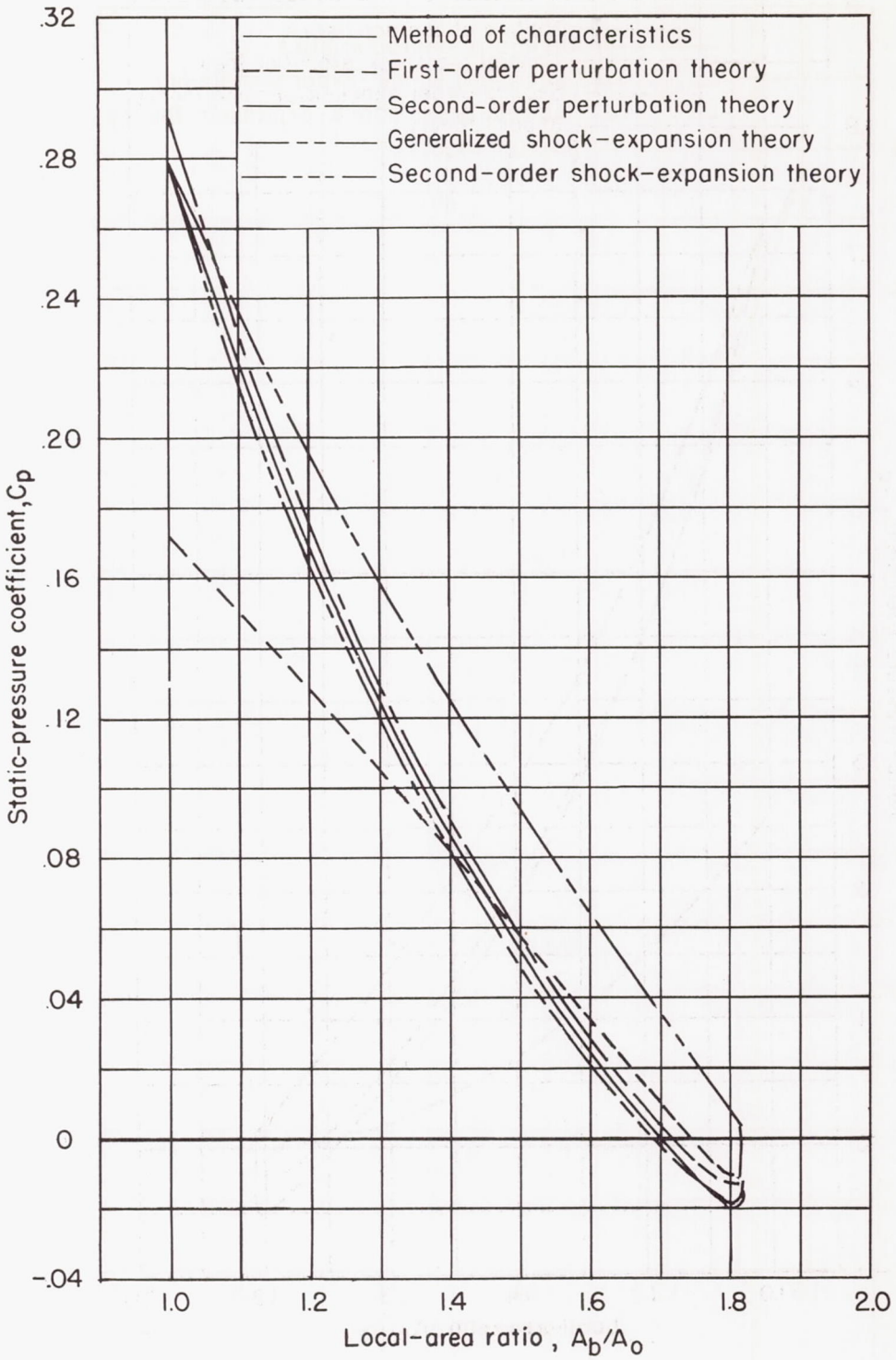

(c) $M_\infty = 2.5$, $\eta = 9$

Figure 10.- Continued.

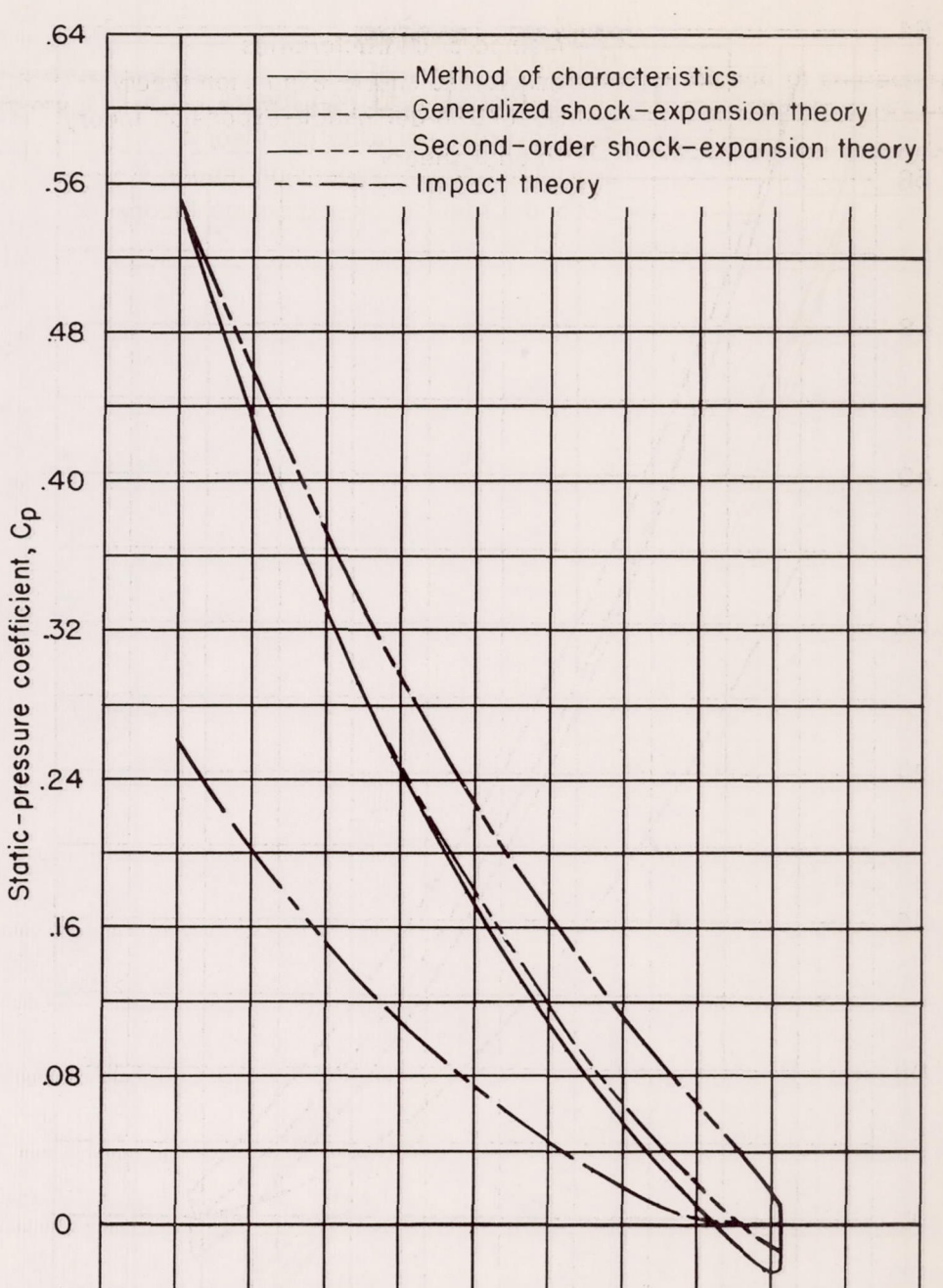

(d) $M_\infty = 2.5$, $\eta = 15$

Figure 10.- Continued.

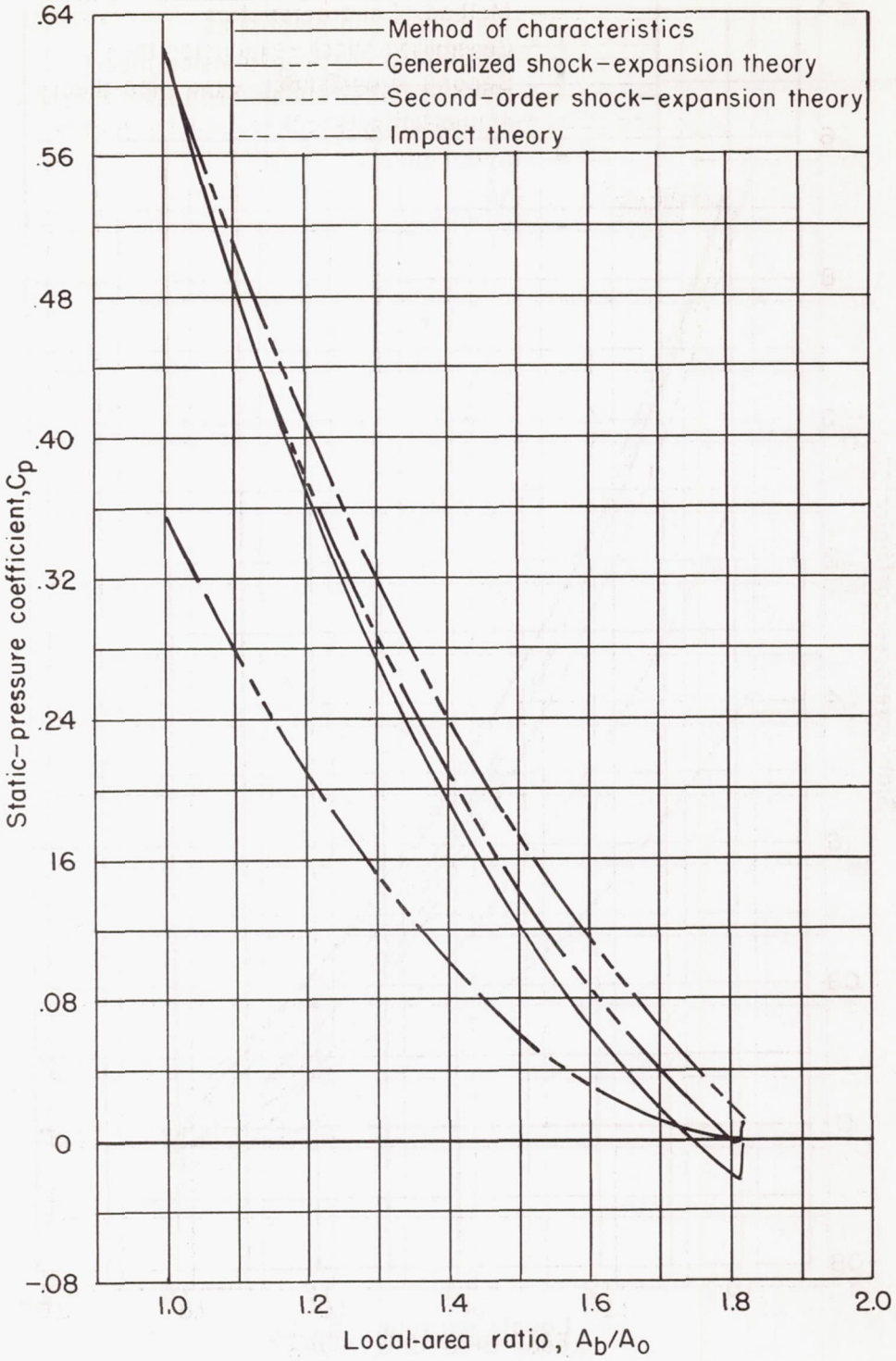

(e) $M_\infty = 3.0$, $\eta = 18$

Figure 10.- Continued.

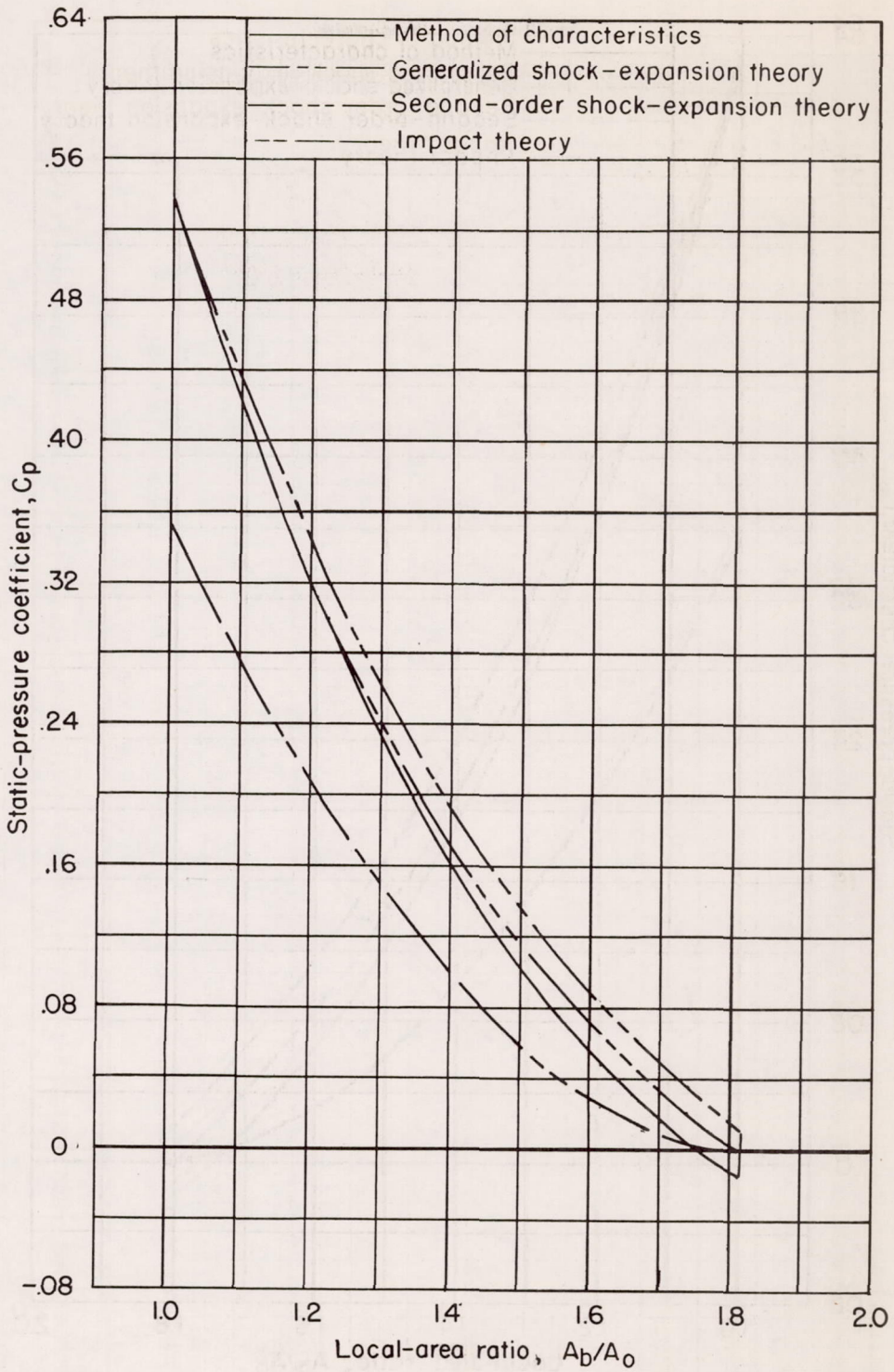

(f) $M_\infty = 4.0$, $\eta = 18$

Figure 10.- Concluded.

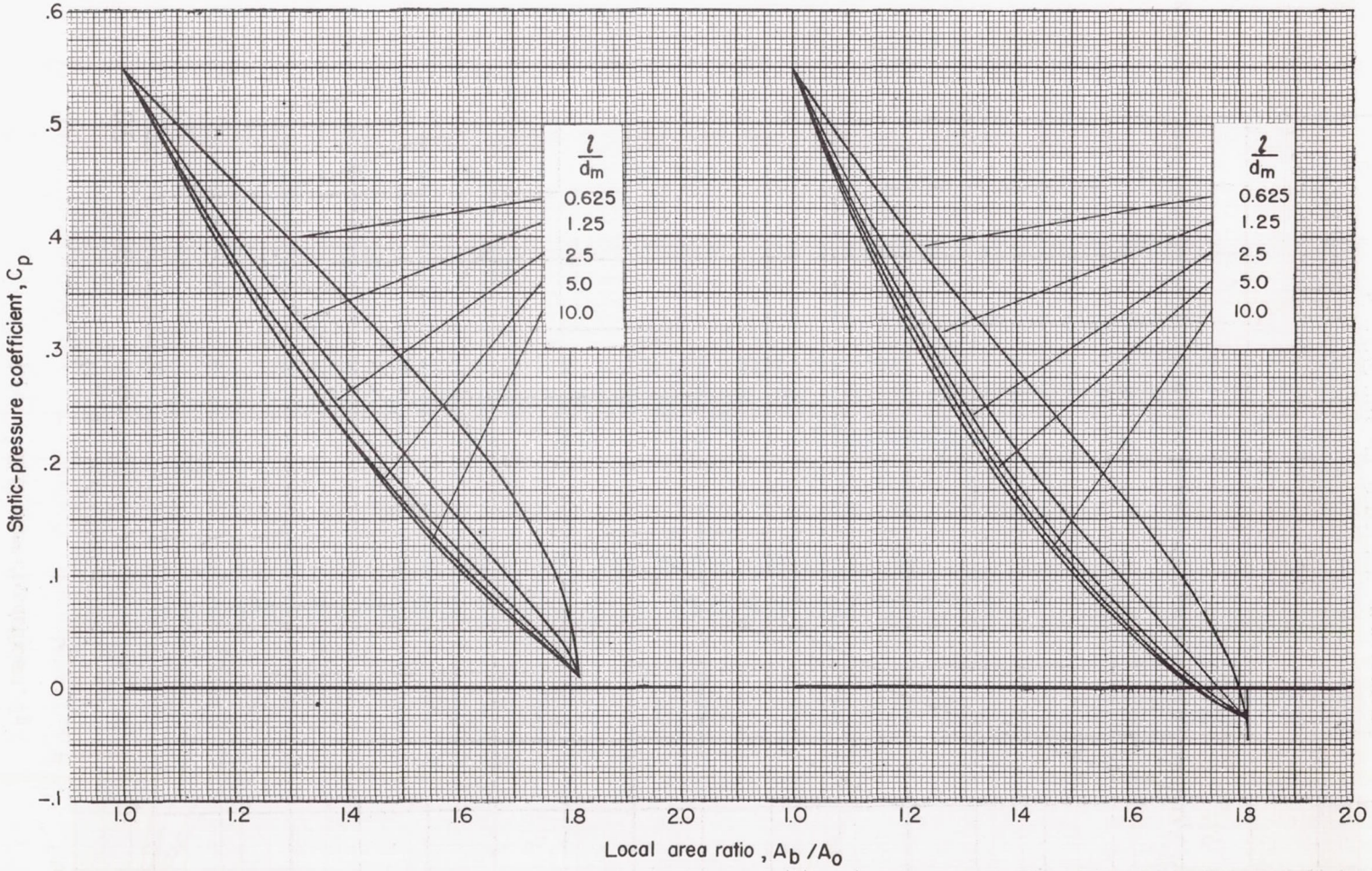

(a) Generalized shock-expansion theory. (b) Method of characteristics.

Figure 11.- The variation of static-pressure coefficient with local-area ratio for bodies of varying fineness ratio; $\delta_o = 21.156^\circ$; $M_\infty = 2.5$; diameter ratio = 0.742.

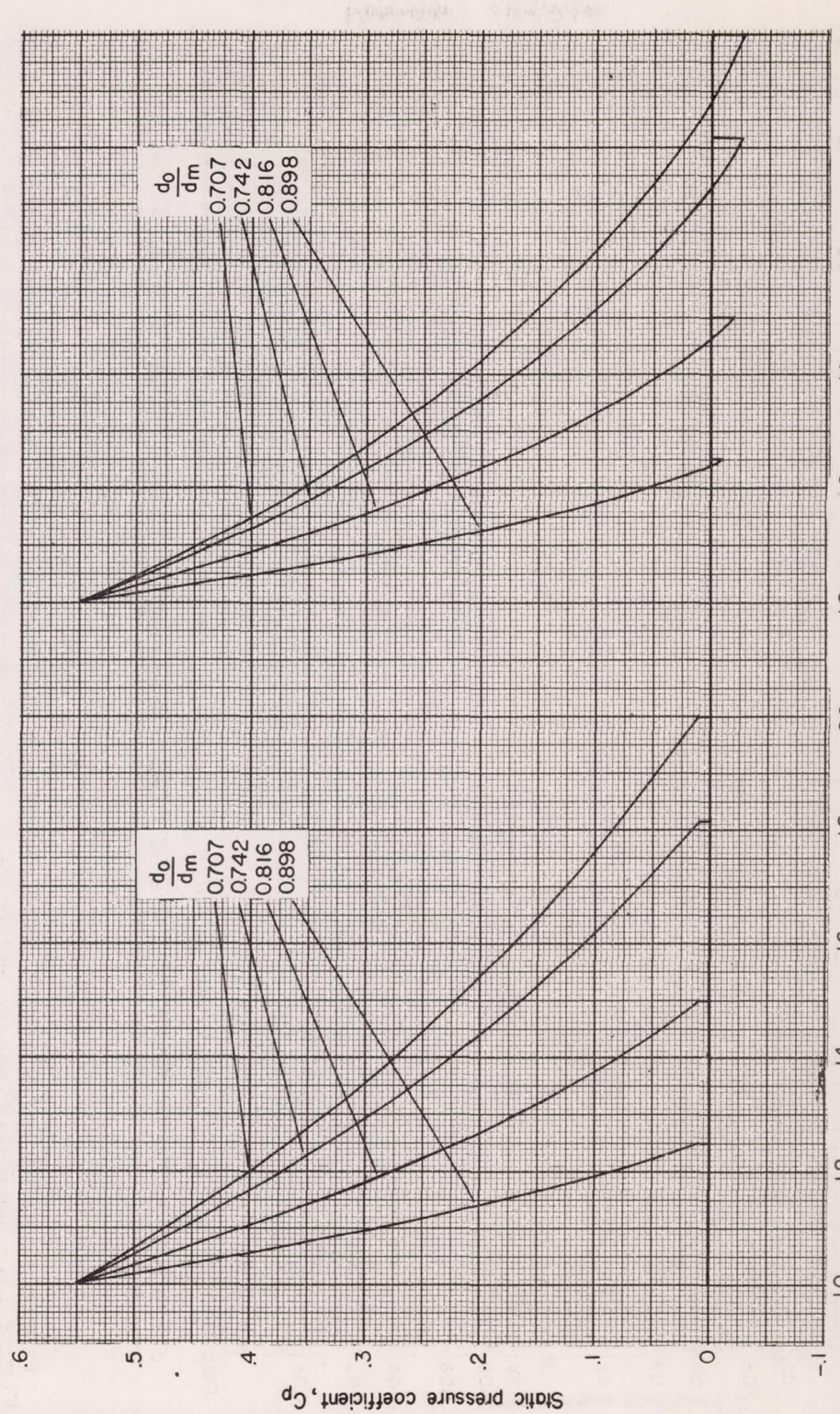

(a) Generalized shock-expansion theory. (b) Method of characteristics.

Figure 12.- The variation of static-pressure coefficient with local-area ratio for bodies of varying diameter ratio; $\delta_o = 21.156$; $M_\infty = 2.5$; fineness ratio = 5.0.

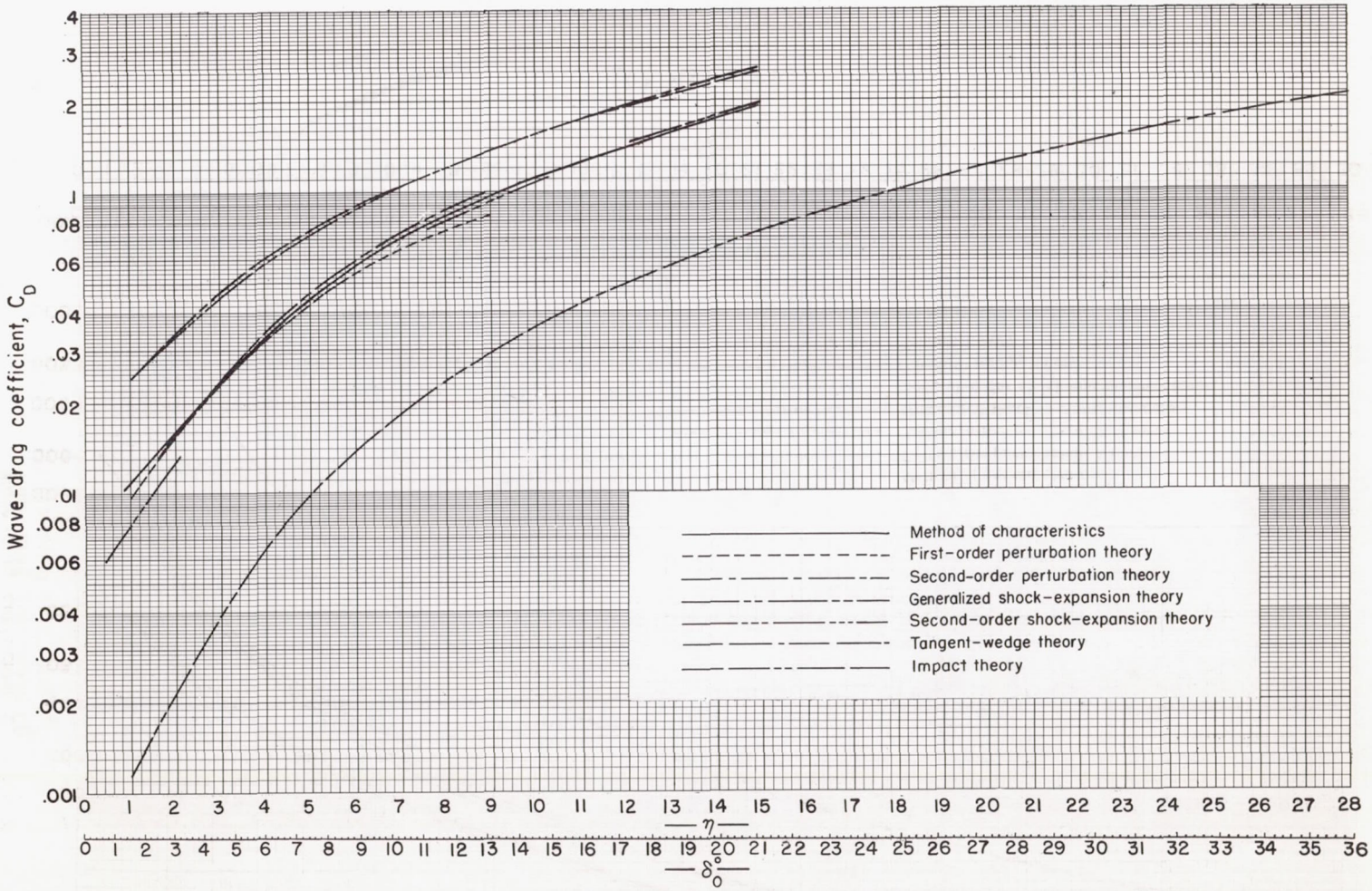

(a) $M_\infty = 2.0$

Figure 13.- The variation of the external wave-drag coefficient as a function of the lip-angle parameters; fineness ratio = 5.0.

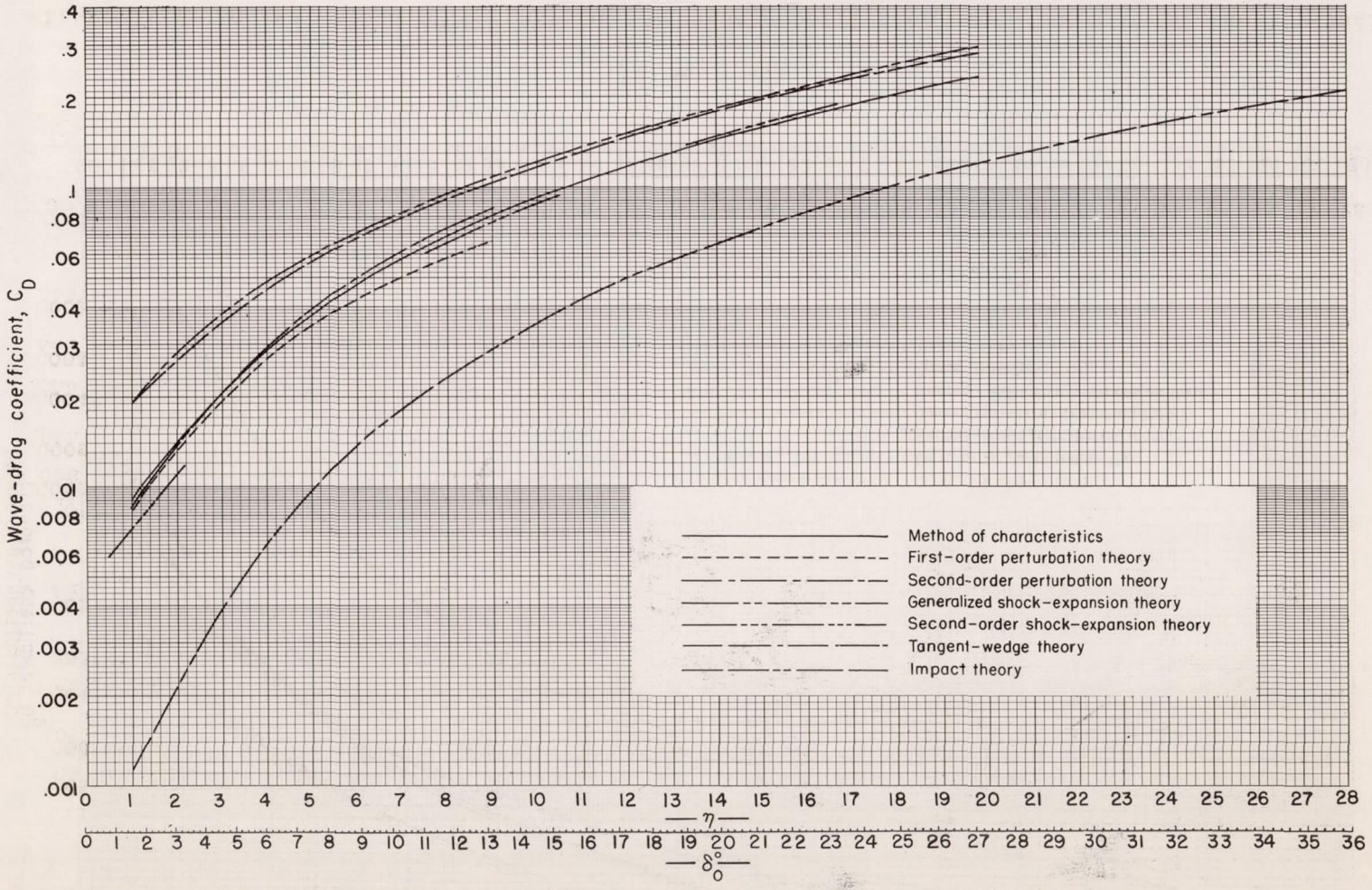

(b) $M_\infty = 2.5$

Figure 13.- Continued.

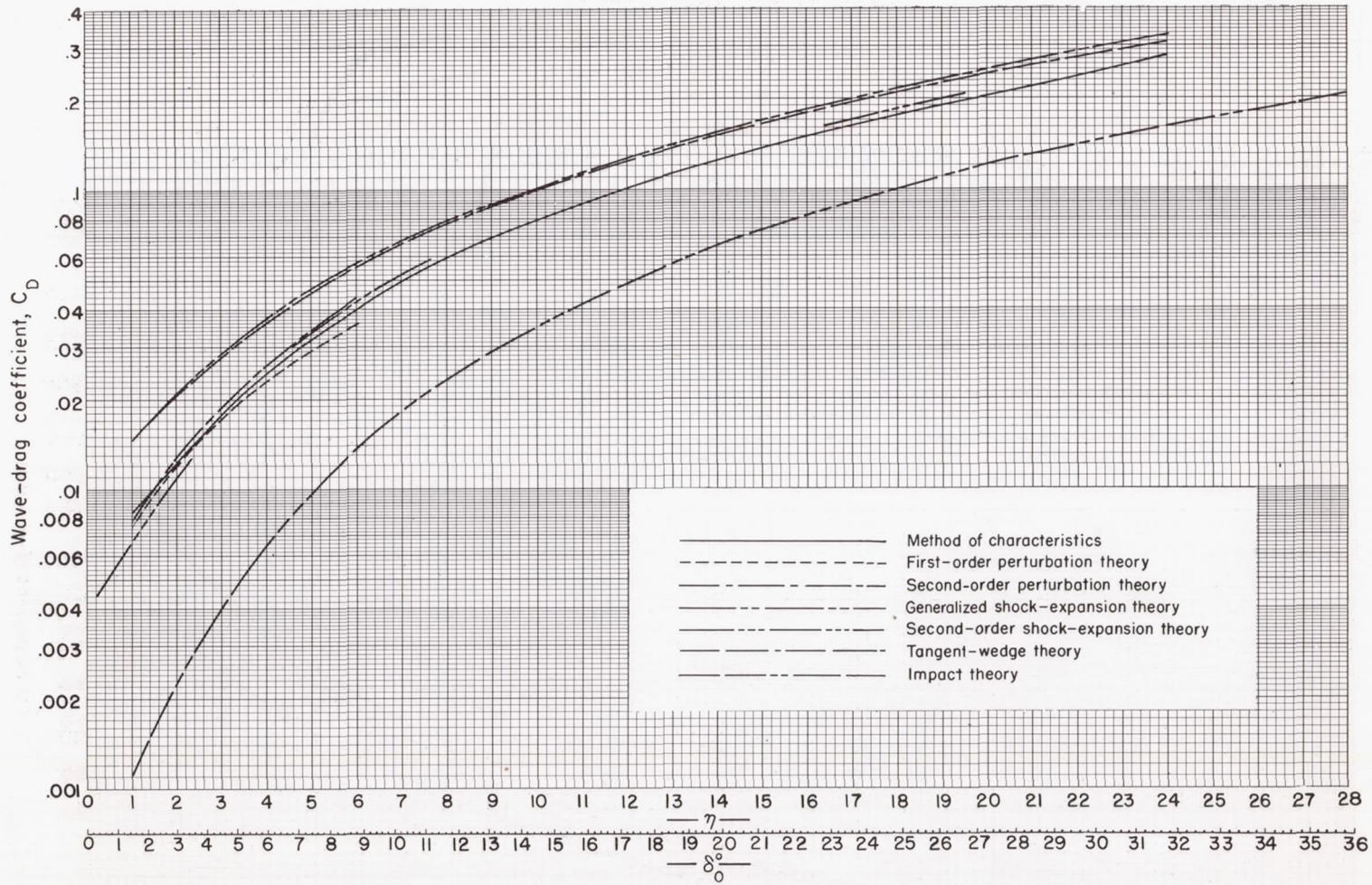

(c) $M_\infty = 3.0$

Figure 13.- Continued.

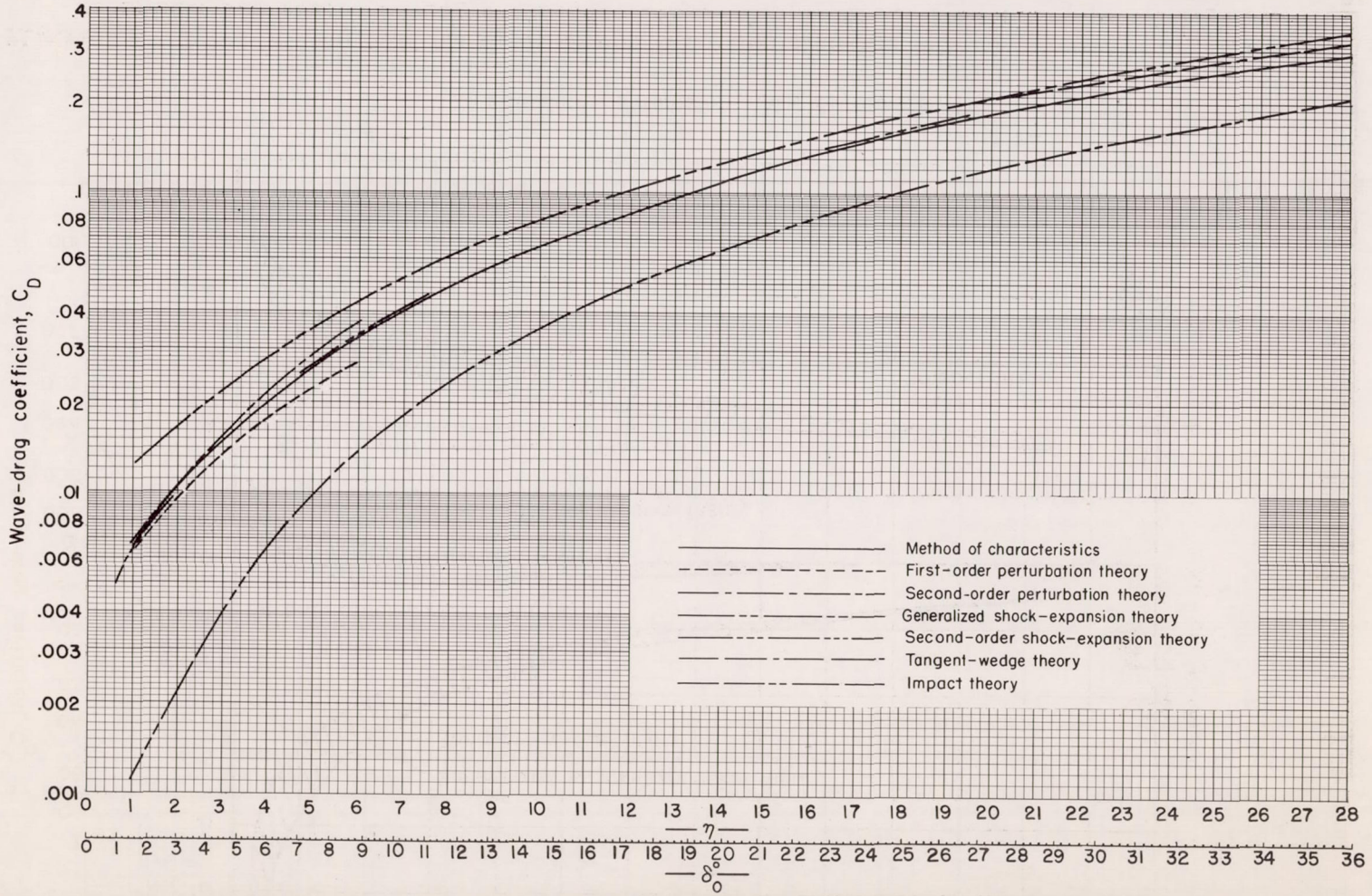

(d) $M_\infty = 4.0$

Figure 13.- Concluded.

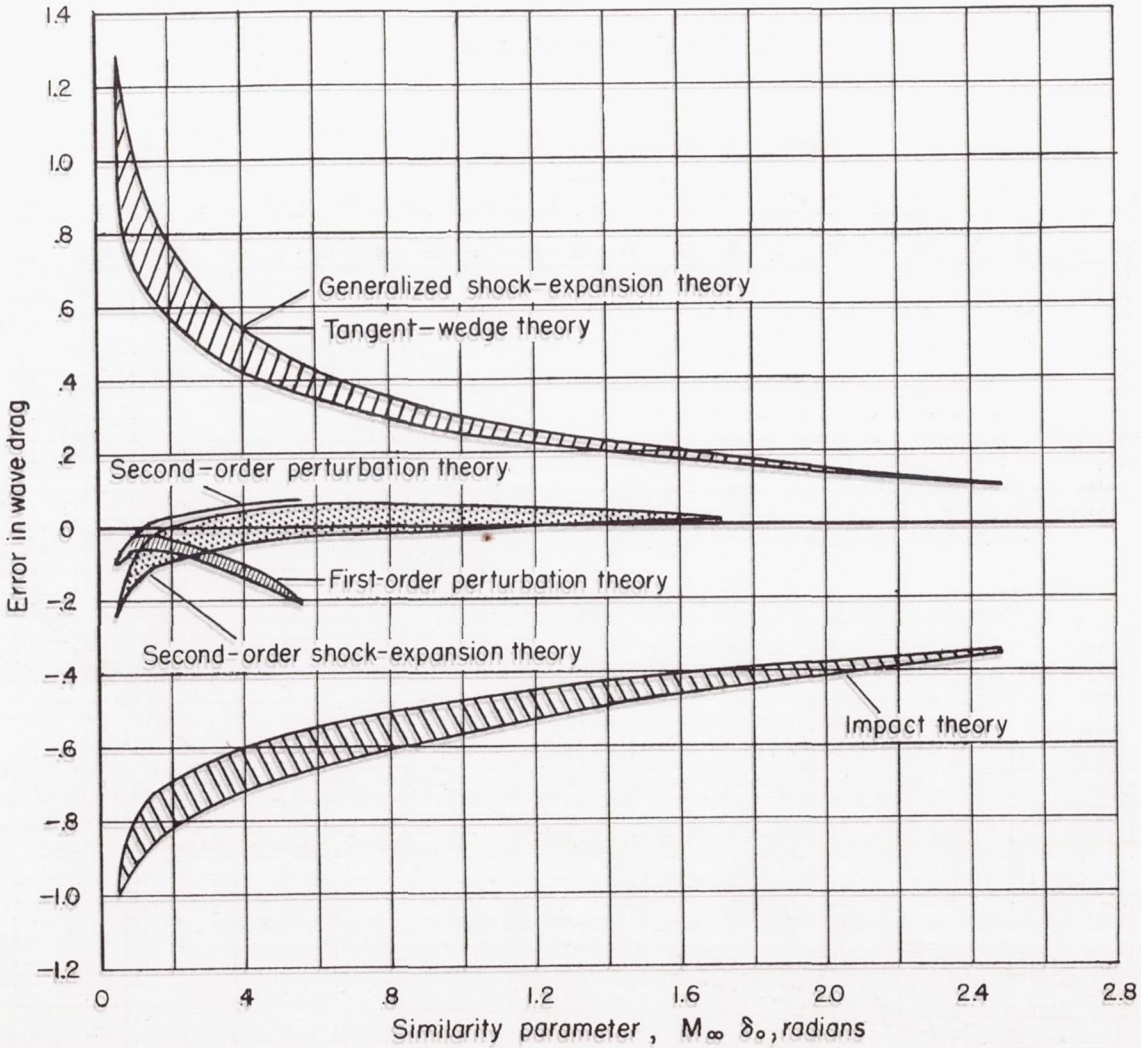

Figure 14.- Error of the various approximate theories with the method of characteristics as a reference for bodies having a fineness ratio of 5.0 and a diameter ratio of 0.742.

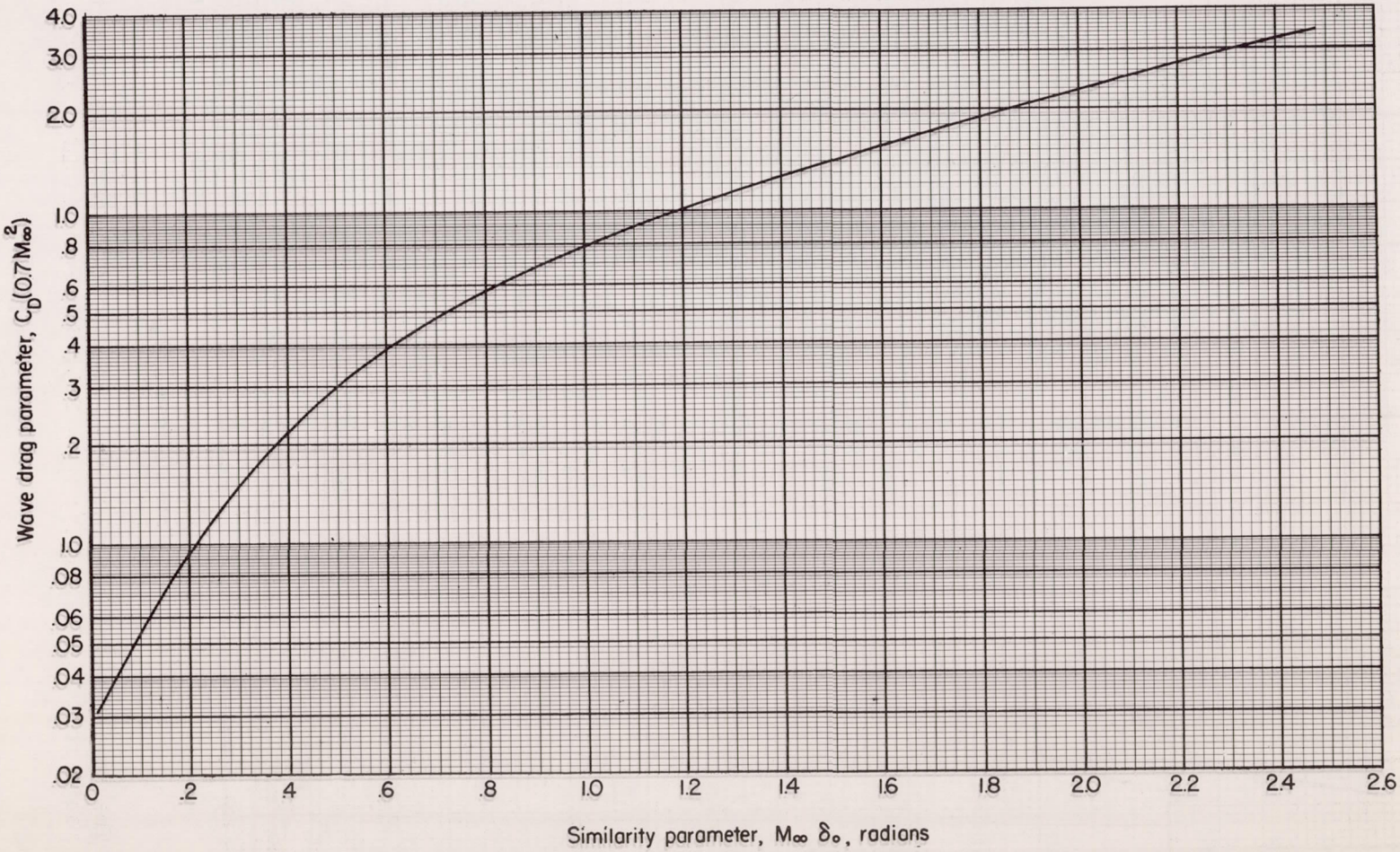

Figure 15.- Correlation of wave-drag coefficients obtained by the method of characteristics for $d_o/d_m = 0.742$ and $l/d_m = 5.0$.

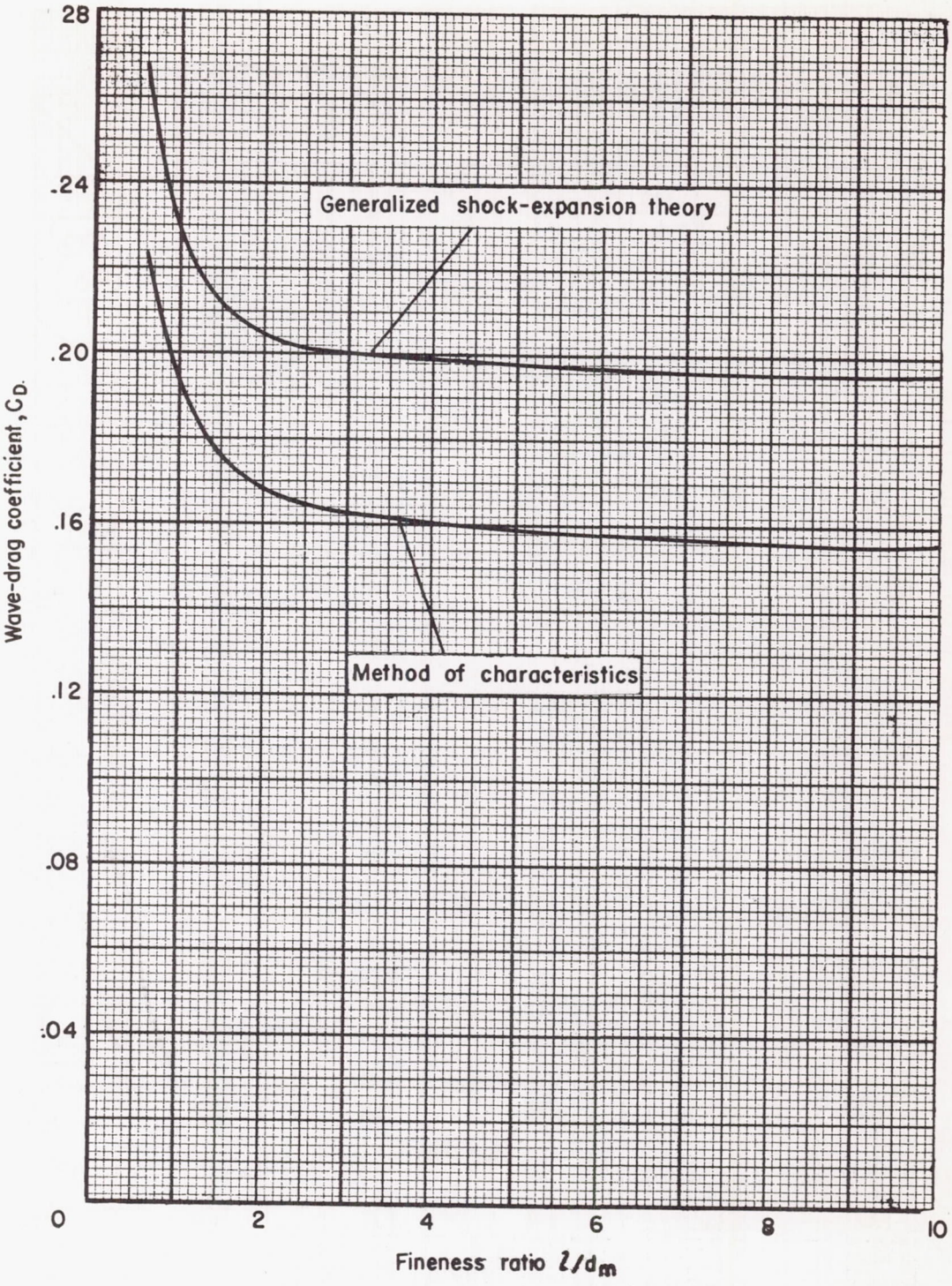

Figure 16.- The variation of external wave-drag coefficient as a function of fineness ratio for $\delta_o = 21.156^\circ$; $M_\infty = 2.5$; diameter ratio = 0.742.

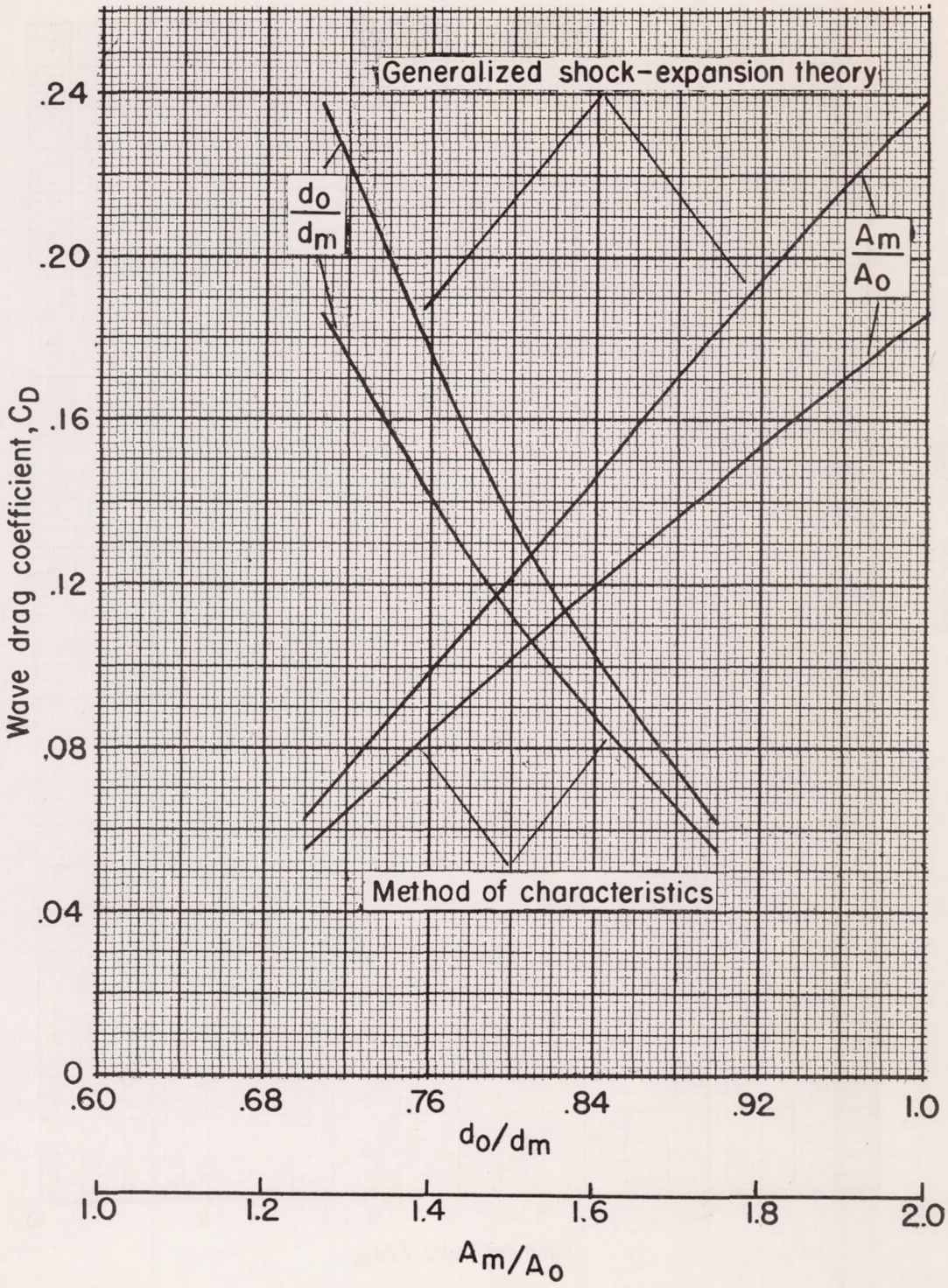

Figure 17.- The variation of external wave-drag coefficient as a function of diameter ratio for $\delta_o = 21.156^\circ$ and $M = 2.5$; fineness ratio = 5.0.